



# RESEARCH MEMORANDUM

WIND-TUNNEL TESTS OF A 0.16-SCALE MODEL OF THE X-3  
AIRPLANE AT HIGH SUBSONIC SPEEDS.- WING AND  
FUSELAGE PRESSURE DISTRIBUTION

By Joseph W. Cleary and Jack A. Mellenthin

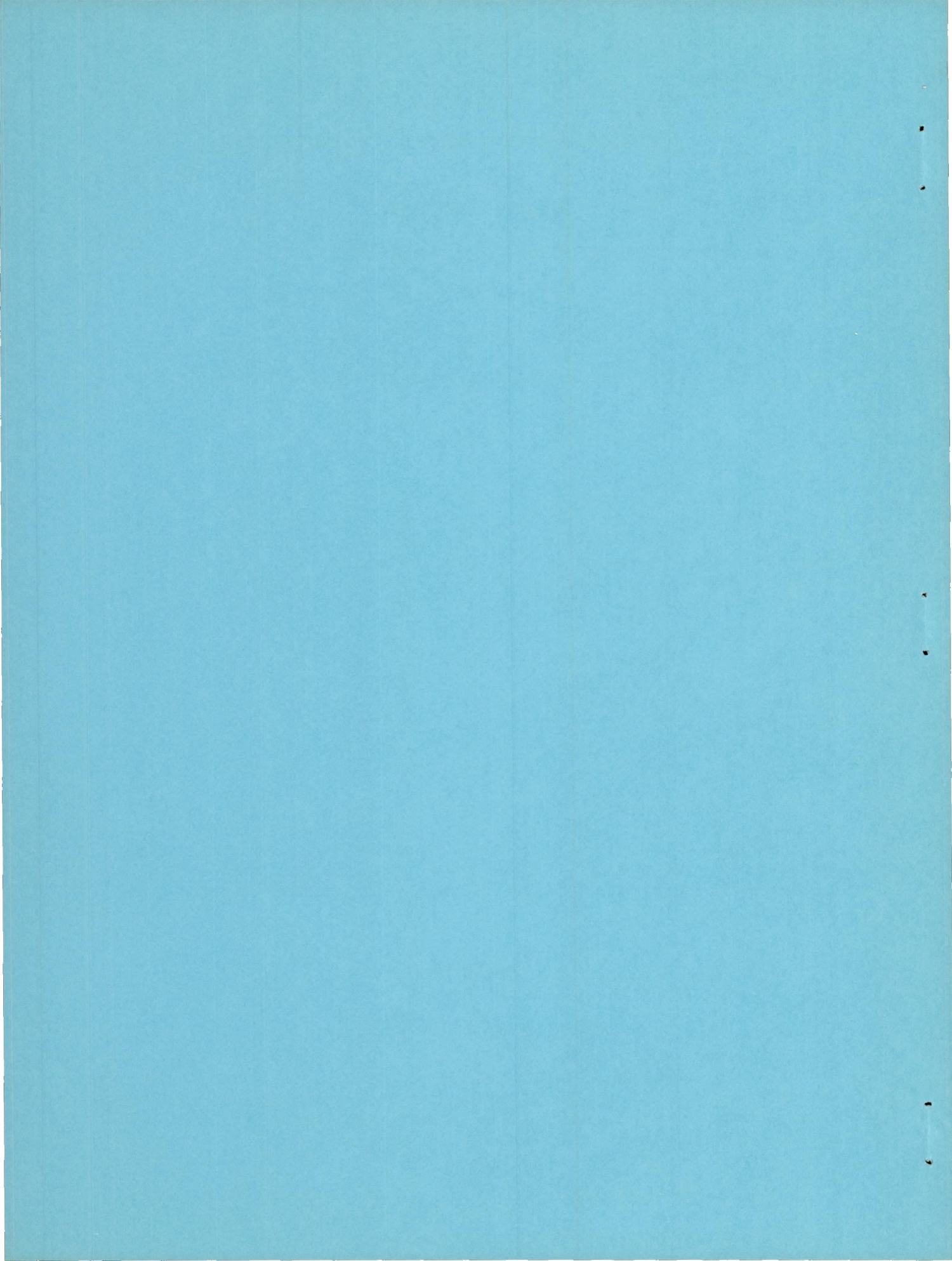
Ames Aeronautical Laboratory  
Moffett Field, Calif.

NATIONAL ADVISORY COMMITTEE  
FOR AERONAUTICS

WASHINGTON

June 22, 1950

Declassified April 15, 1958



NATIONAL ADVISORY COMMITTEE FOR AERONAUTICS

RESEARCH MEMORANDUM

WIND-TUNNEL TESTS OF A 0.16-SCALE MODEL OF THE X-3  
AIRPLANE AT HIGH SUBSONIC SPEEDS.- WING AND  
FUSELAGE PRESSURE DISTRIBUTION

By Joseph W. Cleary and Jack A. Mellenthin

SUMMARY

Measurements of wing and fuselage pressure distributions were made at low and high subsonic Mach numbers on a 0.16-scale model of the projected X-3 research airplane. The tests were conducted in pitch and in yaw and included measurements of the total pressure in the fuselage boundary layer at the location of the left boundary-layer bleed scoop. The X-3 is a supersonic design utilizing a low-aspect-ratio wing and tail.

Pressure-distribution measurements indicated that, although the critical Mach number of the wing was approximately 0.81 at 0° angle of attack, compressibility effects were of little significance below a Mach number of at least 0.90. The principal effect of compressibility was an increase in the pressure gradient over the after 30 percent of the wing chord, causing a tendency for the flow to separate.

At 0.40 Mach number, the wing stalled abruptly at approximately 12° angle of attack. The wing pressure distribution showed this stall was a result of complete separation of the flow from the upper surface of the wing. Deflecting the leading-edge flaps delayed the stall to a higher angle of attack with some increase in the maximum section normal force.

INTRODUCTION

Measurements of wing and fuselage pressure distributions were made on a 0.16-scale model of the X-3 airplane in conjunction with high-speed lateral- and longitudinal-stability tests (references 1 and 2) as it was desired to calculate the chord and span loading, to estimate the critical Mach number of the wing and fuselage combination, and to furnish aerodynamic data of general interest on this supersonic design.

The tests were conducted in the Ames 16-foot high-speed wind tunnel and were made at the request of the U. S. Air Force. The tests extended over a Mach number range from 0.40 to 0.925.

### COEFFICIENTS AND SYMBOLS

The following definitions apply to the coefficients and symbols used in this report:

- $c_n$  section normal-force coefficient  $\left( \frac{\text{section normal force}}{qc} \right)$
- $P$  pressure coefficient  $\left( \frac{p - p_0}{q} \right)$
- $P_{cr}$  critical pressure coefficient (the pressure coefficient at which the local velocity became sonic)
- $b$  wing span, feet
- $S$  wing area, square feet
- $c$  wing chord, feet
- $c_{av}$  average wing chord  $\left( \frac{S}{b} \right)$ , feet
- $\bar{c}$  mean aerodynamic chord of the wing  $\left( \frac{\int_0^{b/2} c^2 dy}{\int_0^{b/2} c dy} \right)$ , feet
- $H$  local total pressure, pounds per square foot
- $H_0$  free-stream total pressure, pounds per square foot
- L.E. leading edge
- $M$  free-stream Mach number
- $M_{cr}$  critical Mach number (the free-stream Mach number for which sonic flow first occurred on the model at the station or point being considered)
- $p$  local static pressure, pounds per square foot
- $p_0$  free-stream static pressure, pounds per square foot

- $q$  free-stream dynamic pressure  $\left(\frac{1}{2}\rho V^2\right)$ , pounds per square foot
- $V$  free-stream velocity, feet per second
- $y$  perpendicular distance along the wing semispan from the plane of symmetry, feet
- $\alpha$  angle of attack of the fuselage reference line corrected for the effects of the tunnel walls, degrees
- $\alpha_u$  angle of attack of the fuselage reference line uncorrected for the effects of the tunnel walls, degrees
- $\delta_{LF}$  leading-edge-flap deflection, positive downward, degrees
- $\rho$  mass density of the free stream, slugs per cubic foot
- $\psi_u$  angle of yaw of the fuselage reference line uncorrected for the effects of the tunnel walls, degrees

#### MODEL AND APPARATUS

Figure 1 shows the locations of the pressure-orifice stations on the wing and fuselage of the model. Pressure-orifice stations on the left wing were 9.02 and 16.56 inches from the plane of symmetry while those on the right wing were 12.16 and 19.20 inches from the same reference plane. The orifices on the fuselage were in longitudinal rows as shown in the sketch. A total-pressure rake was installed on the fuselage at station 43.20 inches to measure the thickness of the boundary layer at a location that corresponded to the entrance of the left boundary-layer bleed scoop. Figures 2, 3, and 4 are photographs of the model and of the installation of the boundary-layer rake.

The 0.16-scale model had an aspect ratio of 3.01 and a wing taper ratio of 0.4. The 75-percent-chord line of the wing was perpendicular to the plane of symmetry. The wing had a symmetrical hexagonal section 4.5 percent thick with rounded corners at 30- and 70-percent chord and sharp leading and trailing edges. Figure 1 shows a typical section through the wing. A detailed description of the model and a table of dimensions are given in reference 1.

The model for all pressure measurements consisted of the wing, the tail, and the fuselage with the tail boom. The canopy, air scoops, and nose fins were omitted.

The model was supported on a sting that carried the pressure leads from the model to mercury-in-glass manometers. Pressure-distribution measurements were made in pitch at  $0^\circ$  angle of yaw and, in yaw, at approximately  $6.2^\circ$  angle of attack. With the model mounted so the wing span was vertical, the angle of yaw was varied with the mechanism normally used to vary the angle of attack. (See fig. 3.) The angles of attack and of yaw of the model were measured visually with a protractor mounted outside the tunnel test section.

### REDUCTION OF DATA

The wind-tunnel-wall and constriction corrections are given in reference 1.

Section normal-force data were derived by mechanical integration of pressure-distribution plots. The section loading coefficients were computed by multiplying the section normal-force coefficients by the ratio of the section chord to the average wing chord.

### RESULTS AND DISCUSSION

#### Characteristics in Pitch

Wing pressure distribution.— The distribution of pressure over the wing of the model with the leading-edge flaps undeflected is shown in figure 5. As the angle of attack was increased, at 0.40 Mach number, the minimum pressure coefficient near the leading edge increased in absolute value up to an angle of attack of approximately  $3^\circ$  to  $6^\circ$ . Further increase in angle of attack extended the region of approximately uniform minimum pressure coefficient on the upper surface until at  $12^\circ$  it covered from 25 to 60 percent of the chord. Between  $12^\circ$  and  $15^\circ$  angle of attack, the flow over the whole upper surface separated and remained separated at the higher angles of attack. The changes in pressure distribution between  $6^\circ$  and  $12^\circ$  angle of attack represent a rearward shift of the center of pressure and appear as a stable variation of the tail-off pitching moment in the data of reference 1.

The effects of compressibility do not appear significant below a Mach number of approximately 0.90. At Mach numbers of 0.90 and 0.925, for a given angle of attack, the pressure gradients were steeper over the after 30 percent of the chord than at the lower Mach numbers. The flow also had a tendency toward earlier separation, a factor which might cause some loss in aileron effectiveness at the higher Mach numbers. (See reference 2.)

Deflecting the leading-edge flaps  $10^\circ$  and  $30^\circ$  (figs. 6 and 7, respectively) created a region of minimum pressure coefficient along the flap hinge line that shifted to the leading edge at the higher angles of attack. At the higher Mach numbers and leading-edge-flap angles the flow tended to separate from the upper surface behind the flap hinge line.

Fuselage pressure distribution.— Figure 8 presents the distribution of pressure over the fuselage. The relatively large negative pressures that occurred in the region of the wing are attributed to the combination of the flow fields of the wing and fuselage. The absolute value of the negative pressure coefficient on the fuselage was less than that on the wing for any given angle of attack. The separation of flow that occurred over the upper surface of the wing for angles of attack greater than  $12^\circ$  did not extend over the center of the fuselage in the region of the wing.

Critical Mach number of wing and fuselage.— The variation of critical Mach number of the wing with angle of attack is presented in figure 9 for leading-edge-flap angles of  $0^\circ$  and  $30^\circ$ . With an angle of attack of  $0^\circ$  and a leading-edge-flap angle of  $0^\circ$ , sonic flow first occurred at wing station 16.56 inches at a Mach number of 0.81. The lowest critical Mach number measured with the flaps undeflected was 0.625 at  $7^\circ$  angle of attack at wing station 9.02 inches.

Deflecting the leading-edge flaps  $30^\circ$  lowered the critical Mach number of the wing throughout the usable angle-of-attack range (fig. 9).

The variation of critical Mach number of the fuselage with angle of attack is presented in figure 10. At  $0^\circ$  angle of attack, the lowest critical Mach number measured on the fuselage was 0.89 on the upper row of fuselage orifices. For angles of attack between  $3^\circ$  and  $17.5^\circ$ , the lowest critical Mach number was measured on the right row of fuselage orifices.

Wing section normal-force and section loading characteristics.— Figure 11 presents the variation of section normal force with angle of attack for leading-edge-flap angles of  $0^\circ$  and  $30^\circ$ . The normal-force characteristics are in agreement with the lift characteristics presented in reference 1. Any spanwise variation of the stalling angle was difficult to detect because of the limited data in the region of the stall. The data indicate that the stall probably occurred almost simultaneously at all stations at 0.40 Mach number.

Deflecting the leading-edge flaps  $30^\circ$  delayed the stall and increased the section normal force at the stall almost 50 percent.

The variation of the section loading coefficient along the span for the wing outboard of station 9.02 inches is given in figures 12 and 13 for leading-edge-flap angles of  $0^\circ$  and  $30^\circ$ , respectively.

Boundary layer at fuselage station 43.2 inches.— Measurements were made to determine the thickness of the boundary layer at the entrance to the left boundary-layer bleed scoop. (See figs. 1 and 4.) The ram-recovery ratio in the boundary layer is shown in figure 14. The boundary-layer thickness was of the order of 0.4 inch at all Mach numbers of the test, and the thickness increased slightly with angle of attack.

#### Characteristics in Yaw

Wing and fuselage pressure distribution.— Figures 15 and 16 show the pressure distribution over the wing and fuselage, respectively, for several angles of yaw and an angle of attack of approximately  $6.2^\circ$ .

At  $0^\circ$  yaw and approximately  $6.2^\circ$  angle of attack, peak pressures at the leading edge (primarily at wing station 12.16 inches) were more negative when the model was mounted with the wing span vertical for the yaw tests (fig. 3) than with the model upright for the pitch tests. A contributing factor may have been that, with the model mounted for yaw tests, the wing plane was much nearer to one of the tunnel walls than for tests with the model in the normal attitude. This was due to the fact that the tunnel is but 12 feet wide and the model was not on the tunnel center line. For this reason the pitch data may be the more reliable.

Boundary layer at fuselage station 43.2 inches.— The ram-recovery ratio in the boundary layer at a position corresponding to the entrance to the left boundary-layer bleed scoop with the model yawed is presented in figure 17. The boundary-layer thickness appeared to decrease with increasing angle of yaw. For high angles of yaw, the slight deficiency in ram recovery outside the boundary layer apparently was due to the inability of the rake to measure the full total pressure for the highly yawed attitudes. The data indicate that with the model mounted for yaw tests but with  $0^\circ$  yaw, the boundary layer was slightly thicker than with the model upright at a corresponding angle of attack. The differences may have been due to variations in the surface condition of the model or to inaccuracies of measurement.

#### CONCLUDING REMARKS

Wing and fuselage pressure-distribution measurements on a 0.16-scale model of the proposed X-3 research airplane indicated that, although the critical Mach number was 0.81 at  $0^\circ$  angle of attack, compressibility did not seriously affect the flow over the model below a Mach number of

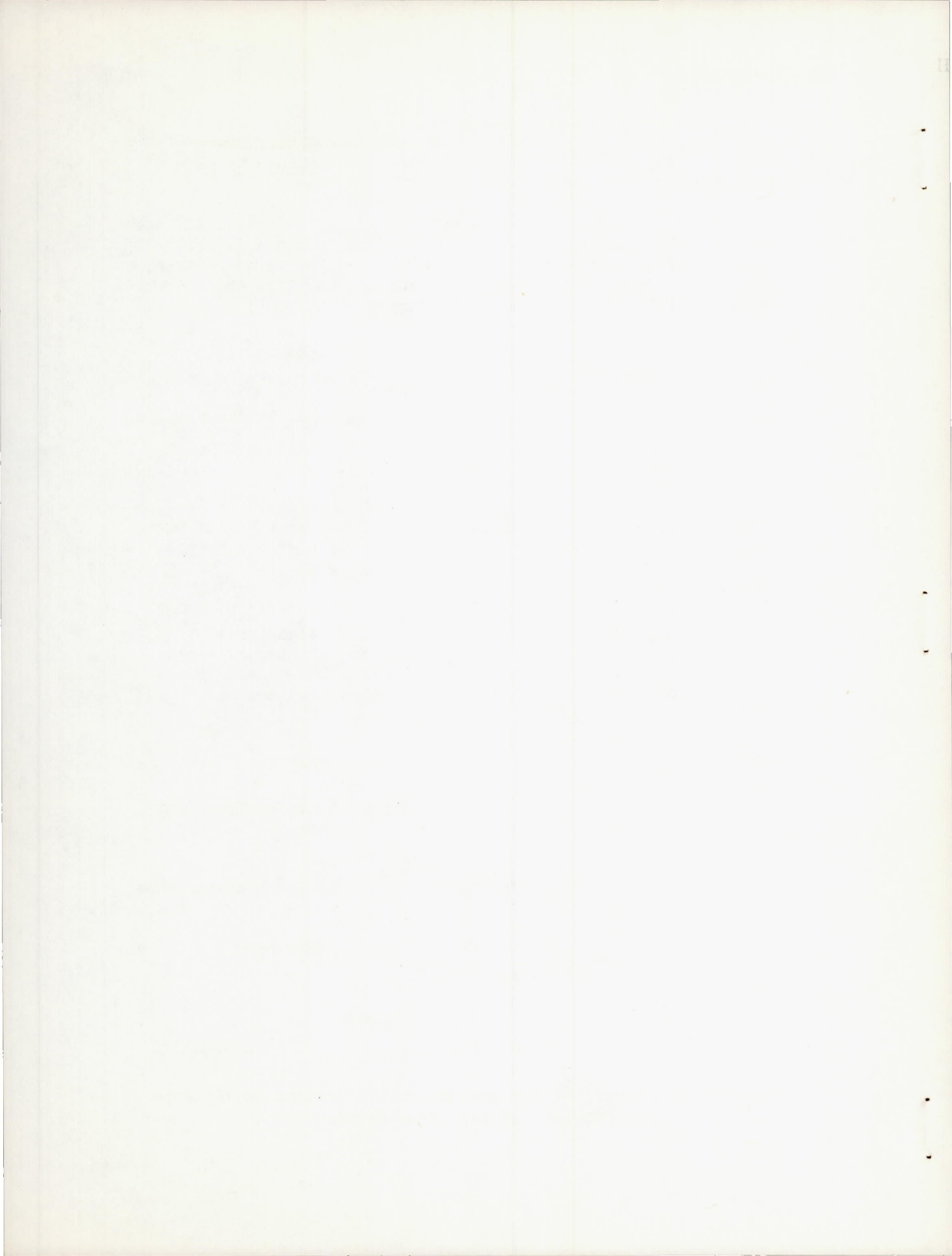
0.90. The principal Mach number effect was to increase the pressure gradient over the after 30 percent of the wing chord, causing a tendency for the flow to separate.

At 0.40 Mach number, the wing stalled at approximately  $12^\circ$  angle of attack. This stall appeared, from the wing pressure distribution, to involve complete separation of the flow from the upper surface. Deflecting the leading-edge flaps  $30^\circ$  delayed the stall and increased the section normal force at the stall almost 50 percent.

Ames Aeronautical Laboratory,  
National Advisory Committee for Aeronautics,  
Moffett Field, Calif.

#### REFERENCES

1. Hamilton, William T., and Cleary, Joseph W.: Wind-Tunnel Tests of a 0.16-Scale Model of the X-3 Airplane at High Subsonic Speeds.— Stability and Control Characteristics.  
NACA RM A50A03, 1950.
2. Cleary, Joseph W., and Mellenthin, Jack A.: Wind-Tunnel Tests of a 0.16-Scale Model of the X-3 Airplane at High Subsonic Speeds.— Additional Stability and Control Characteristics and the Aerodynamic Effects of External Stores and Ram Jets.  
NACA RM A50C30, 1950.



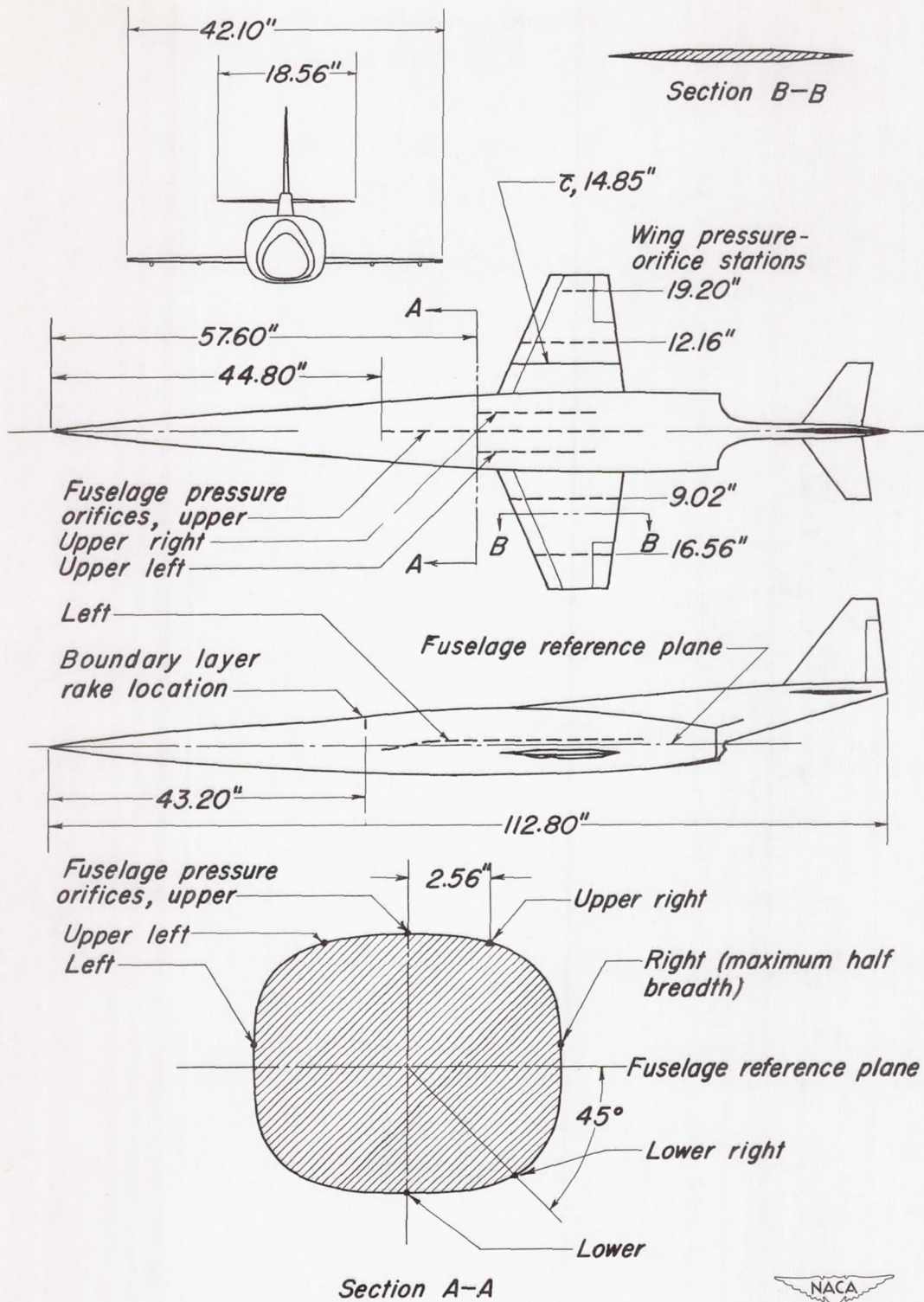
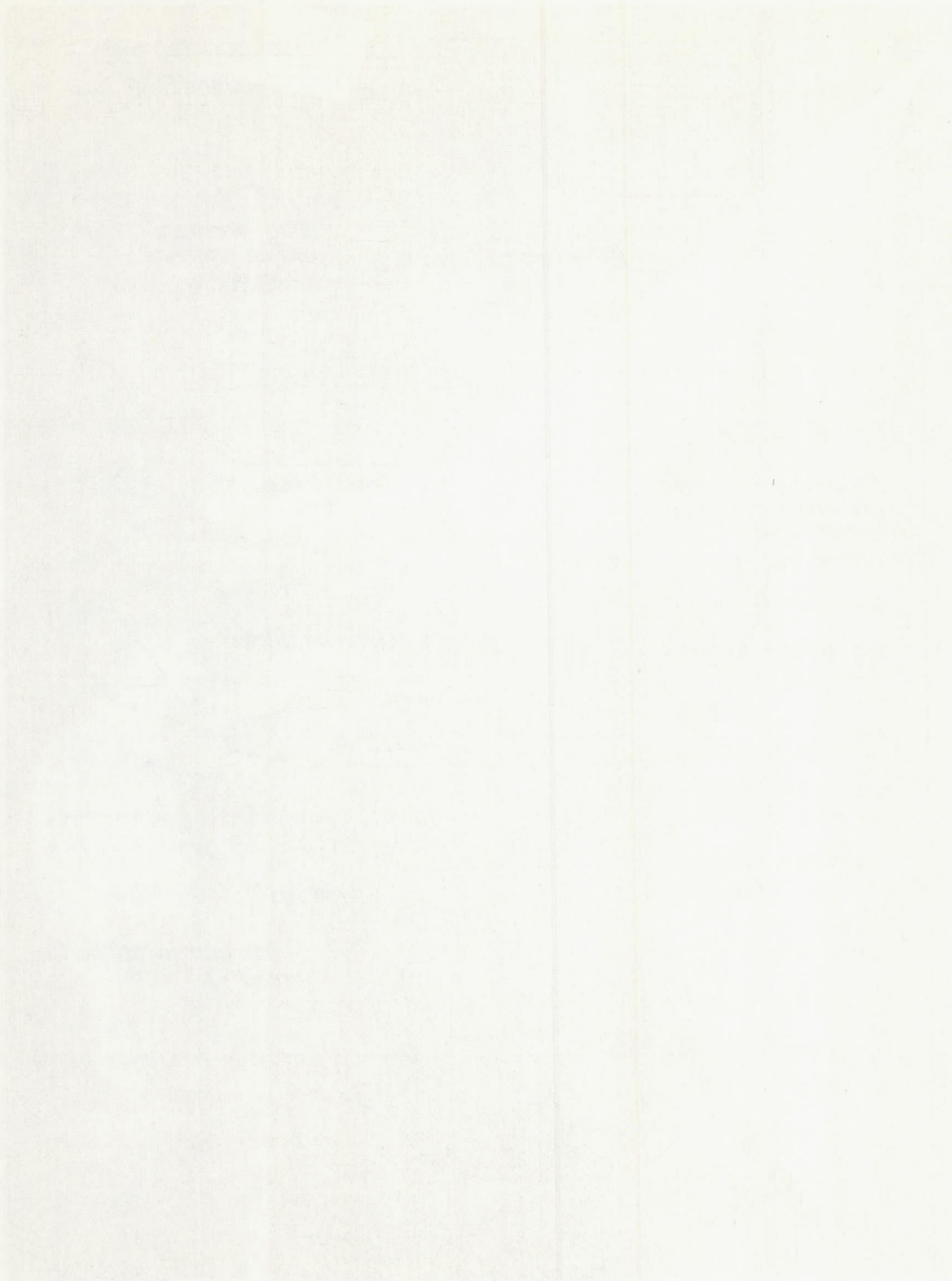


Figure 1.-The location of the pressure-orifice stations on the wing and fuselage of the X-3 model.





Faint, illegible text at the bottom of the page, possibly a footer or a page number.

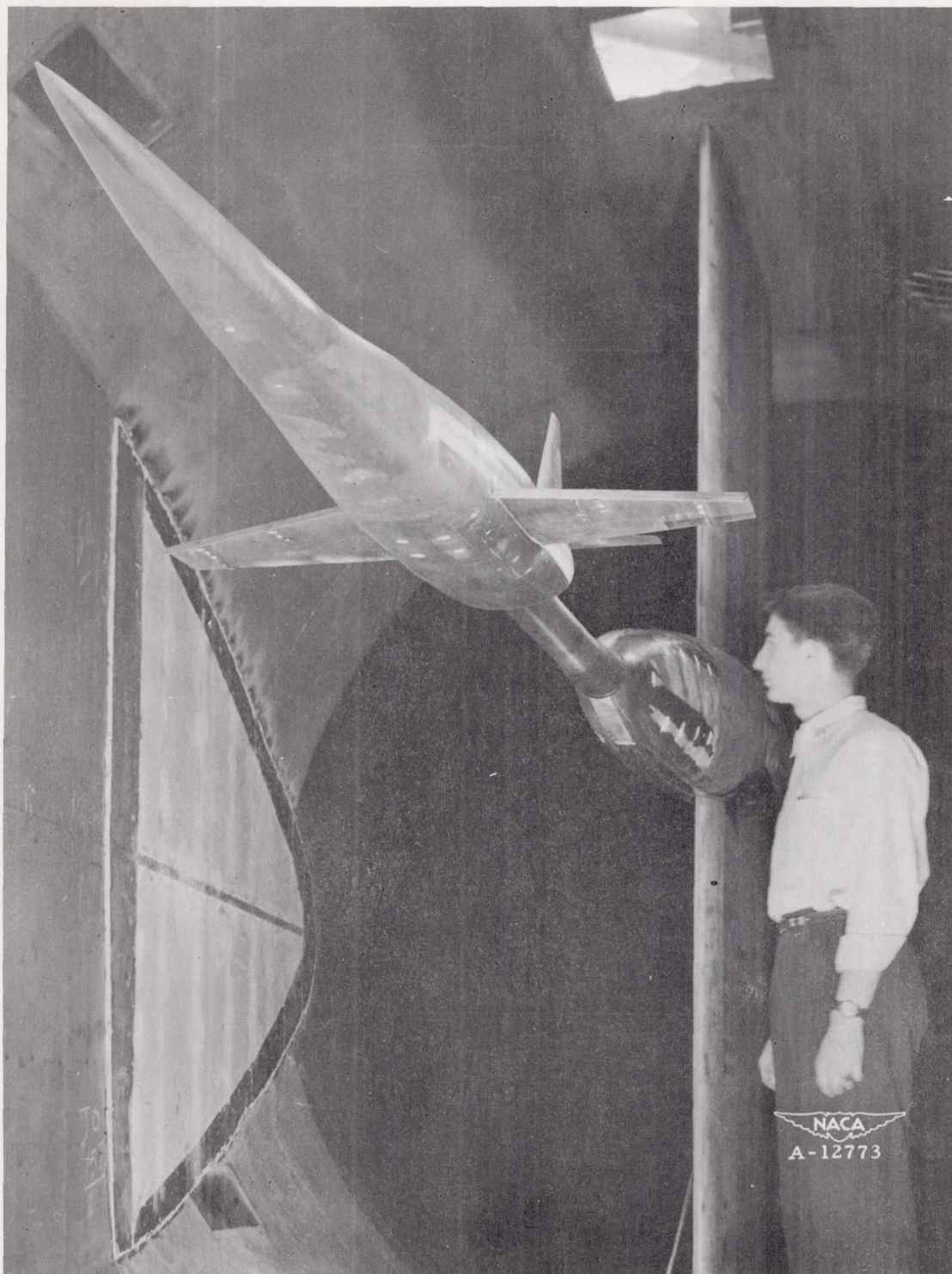


Figure 2.— The X-3 model mounted in the Ames 16-foot high-speed wind tunnel for pressure-distribution tests in pitch.

Faint, illegible text, possibly bleed-through from the reverse side of the page. The text is arranged in several paragraphs and is too light to transcribe accurately.



Figure 3.- The X-3 model mounted in the Ames 16-foot high-speed wind tunnel for pressure-distribution tests in yaw.

1950-1951 - The results of the survey of the I-3 model.

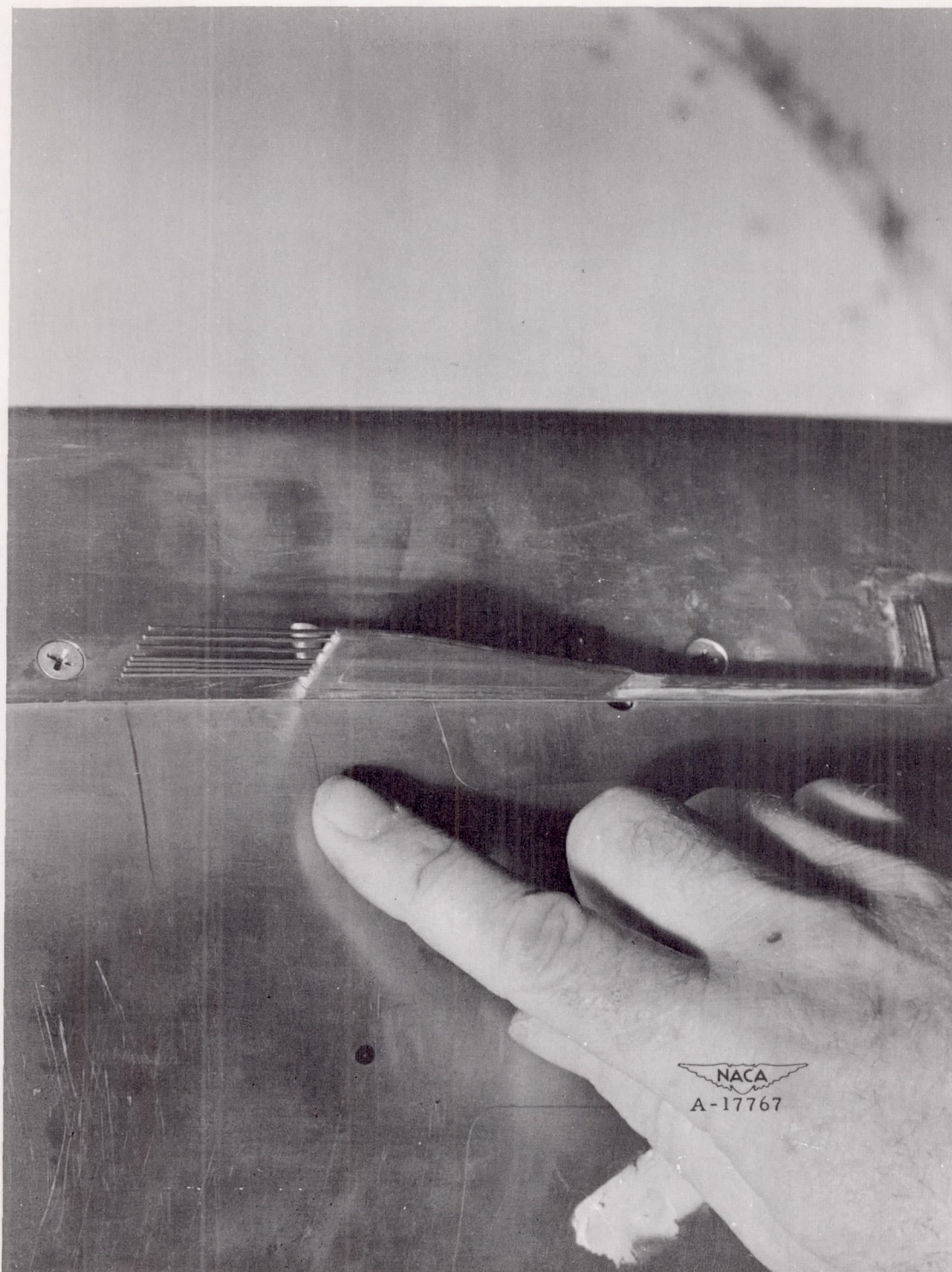
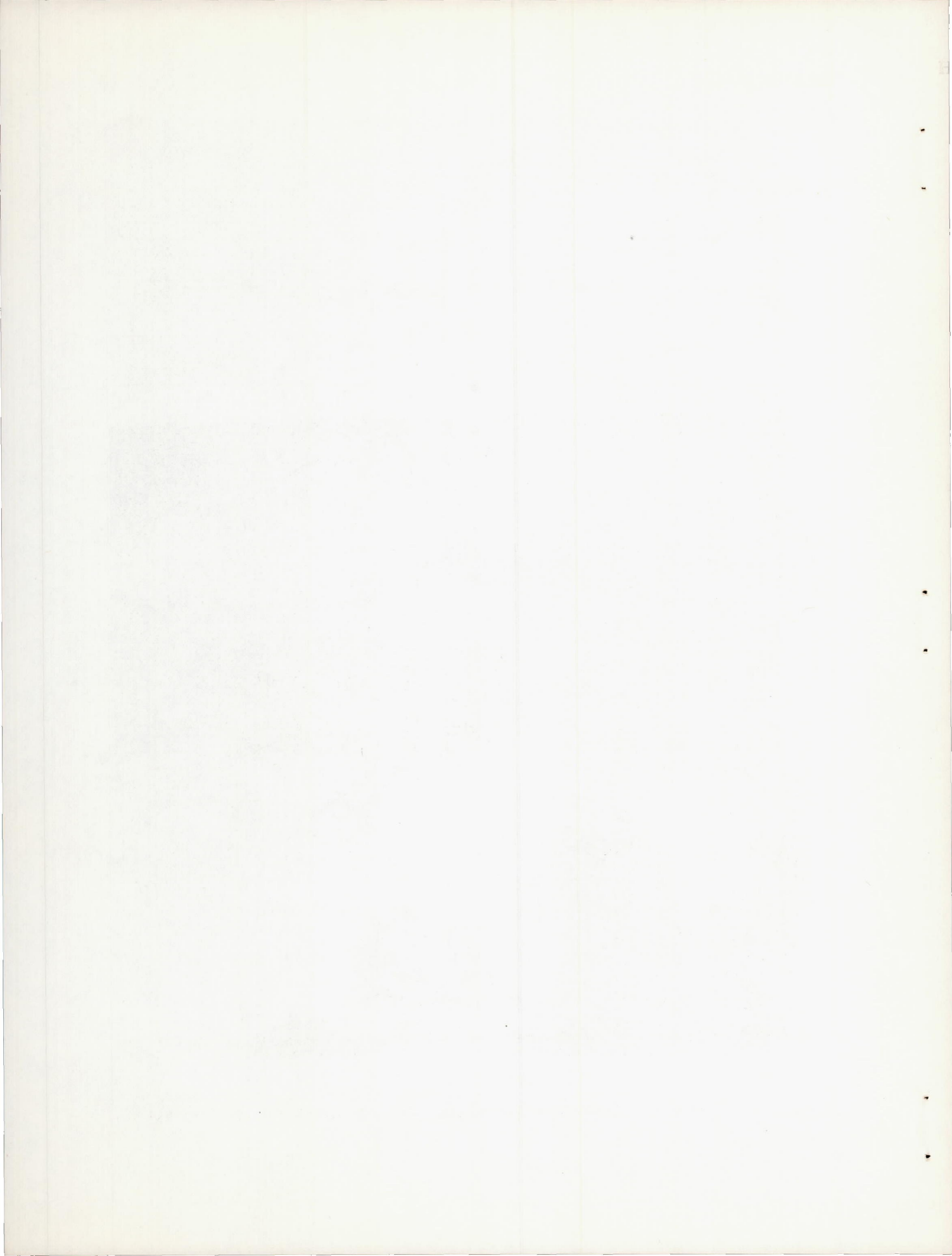


Figure 4.- The fuselage boundary-layer rake mounted on the X-3 model.



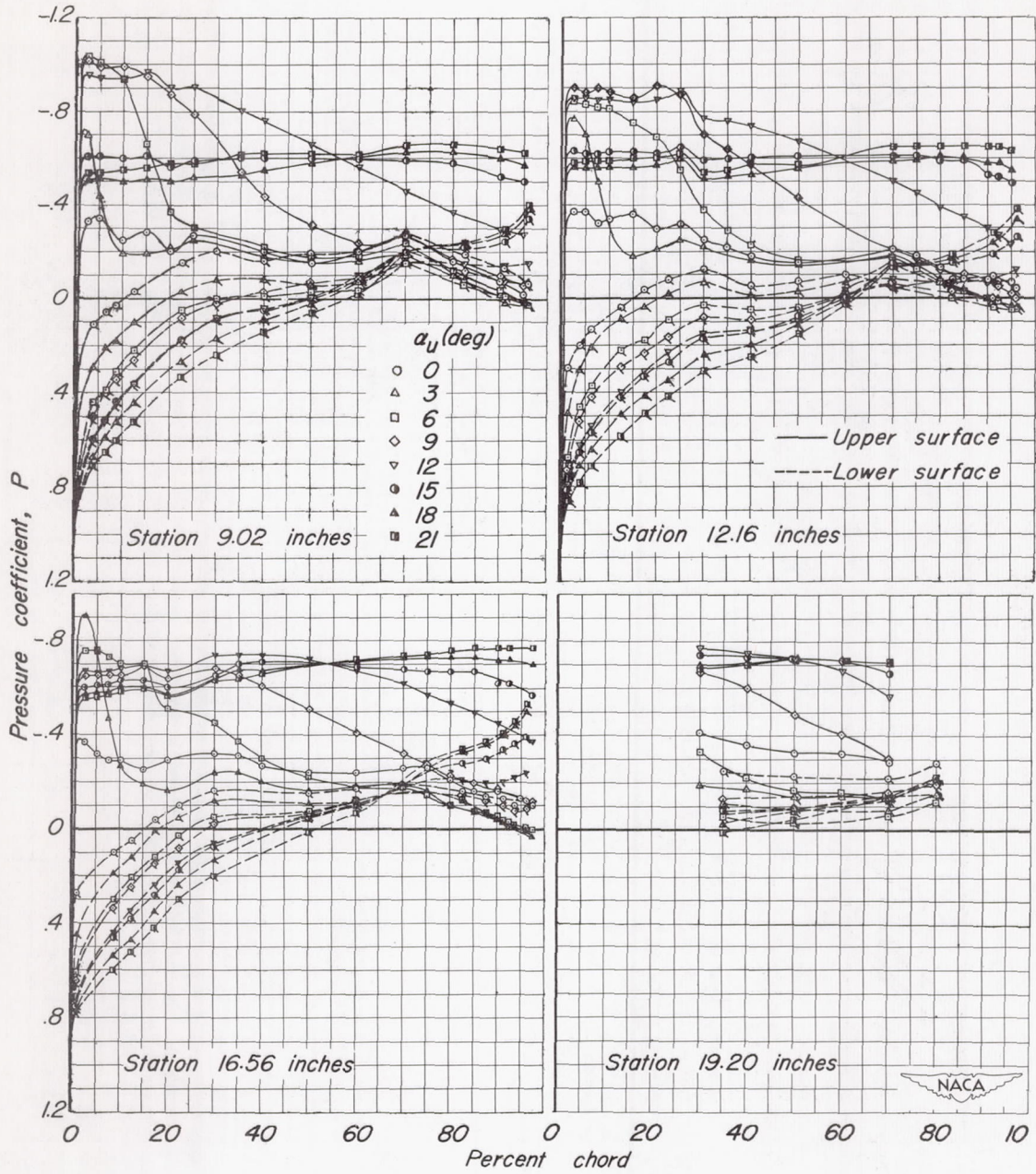
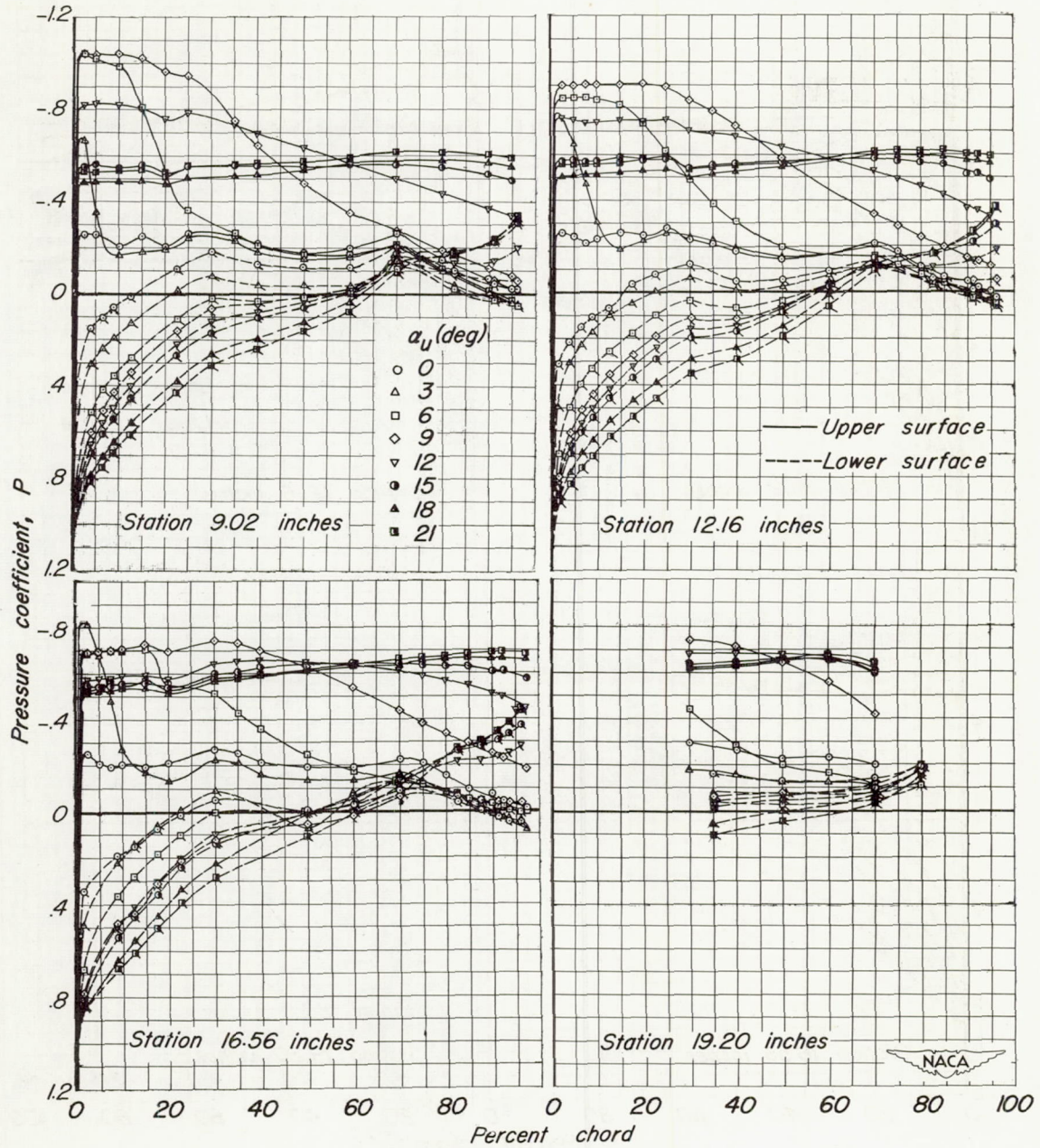
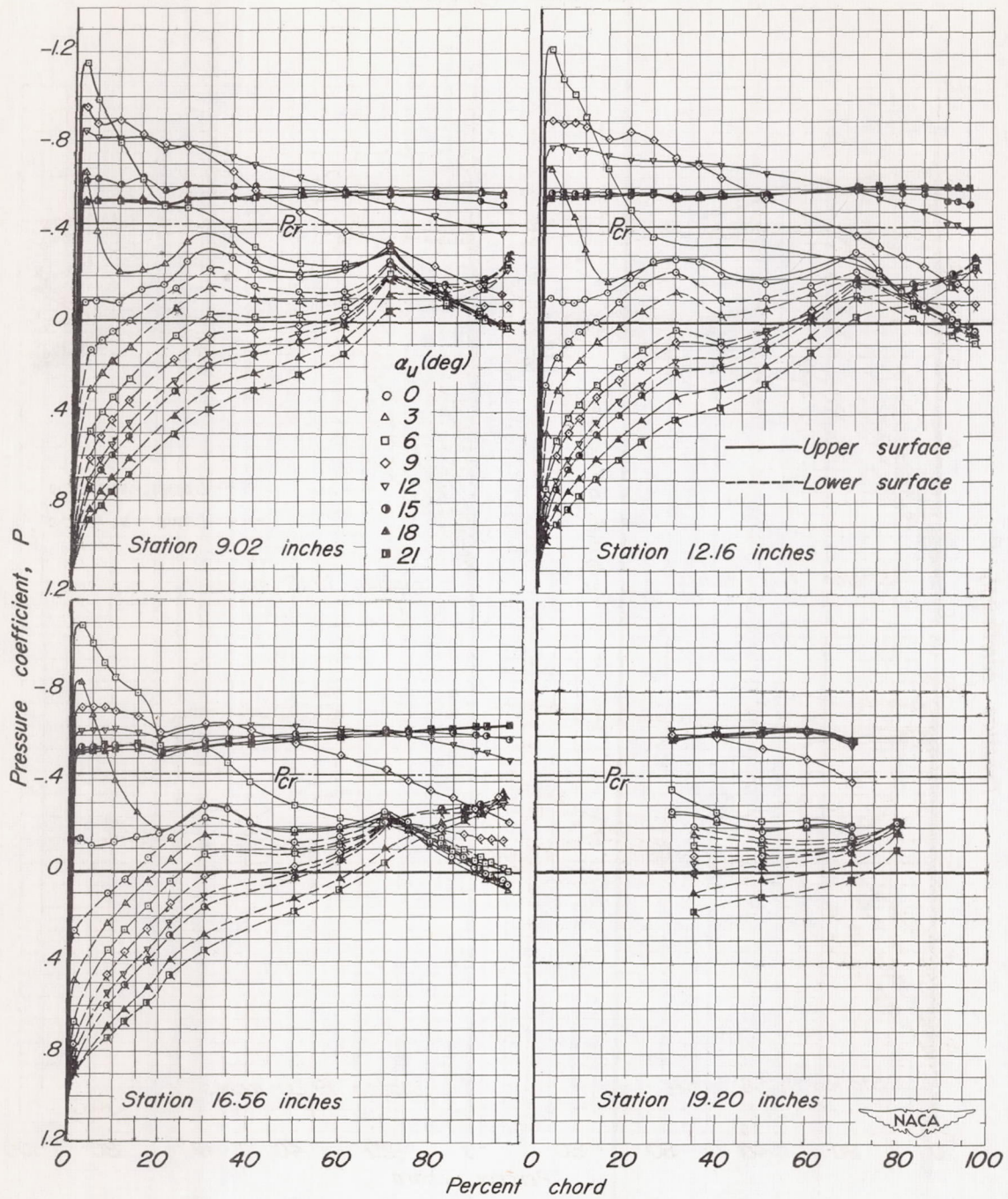


Figure 5.-The pressure distribution over the wing of the X-3 model.  $\psi_0, 0^\circ$ ;  $\delta_{lf}, 0^\circ$



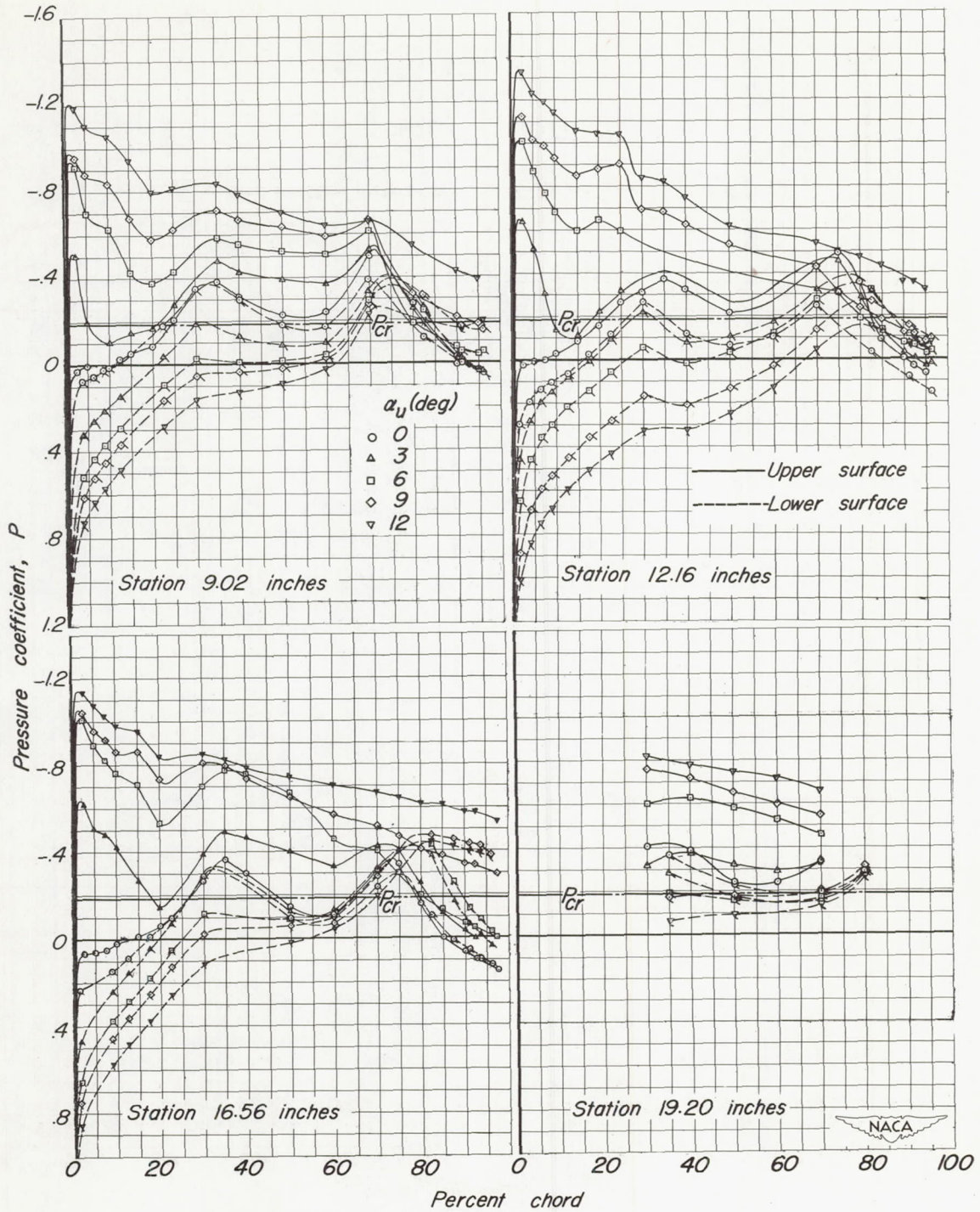
(b) Mach number, 0.60.

Figure 5—Continued.



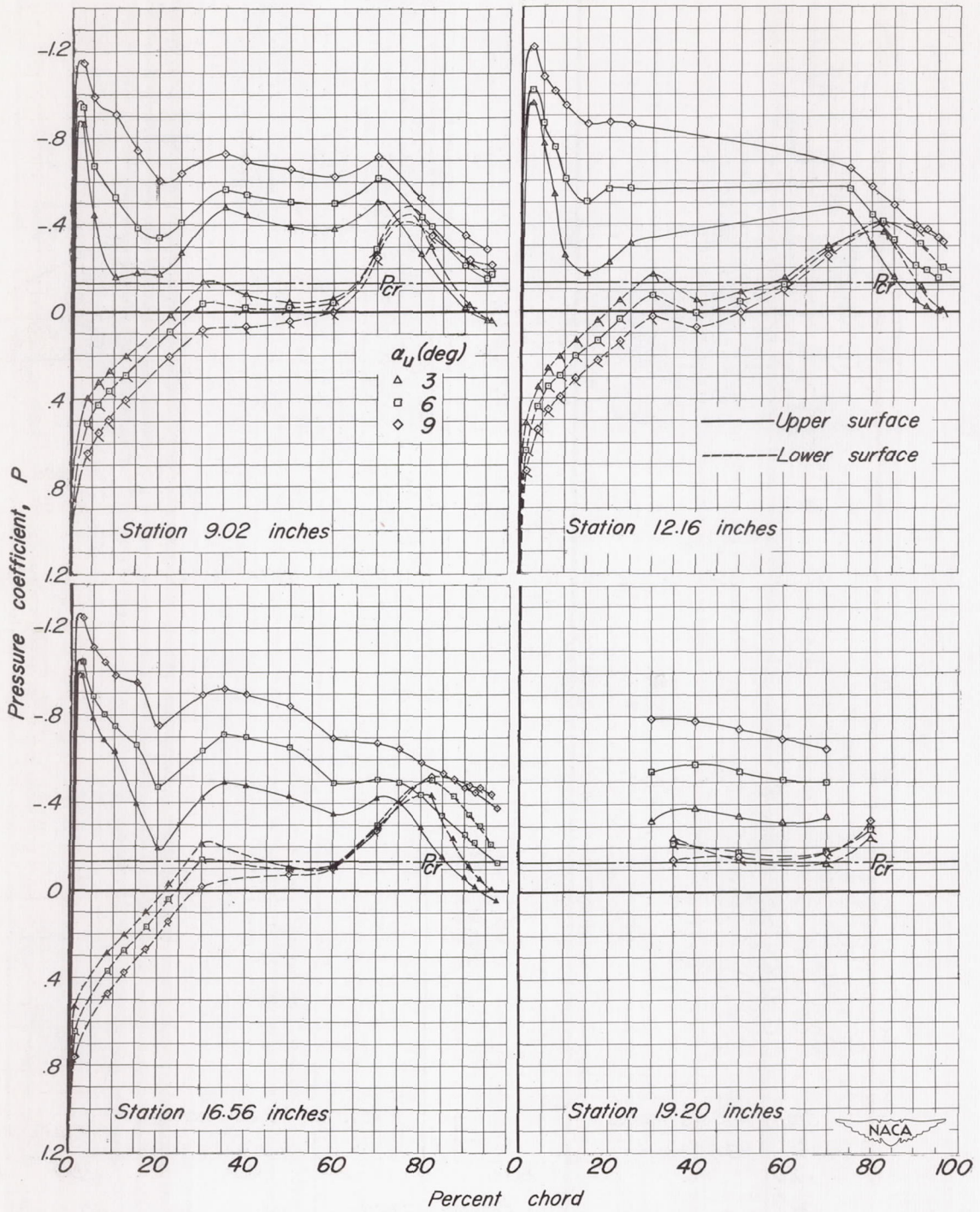
(c) Mach number 0.80.

Figure 5-Continued.



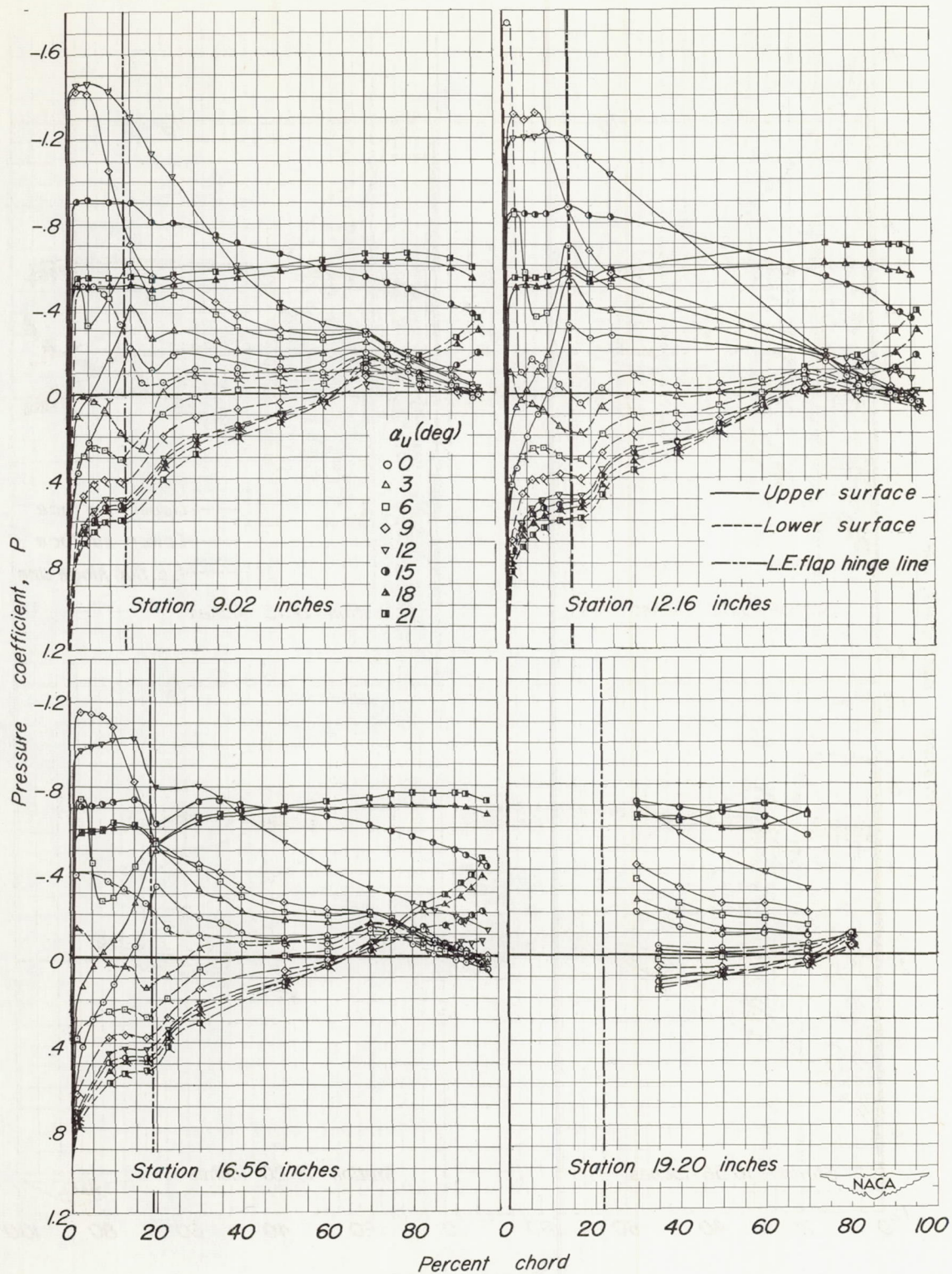
(d) Mach number, 0.90.

Figure 5.-Continued.



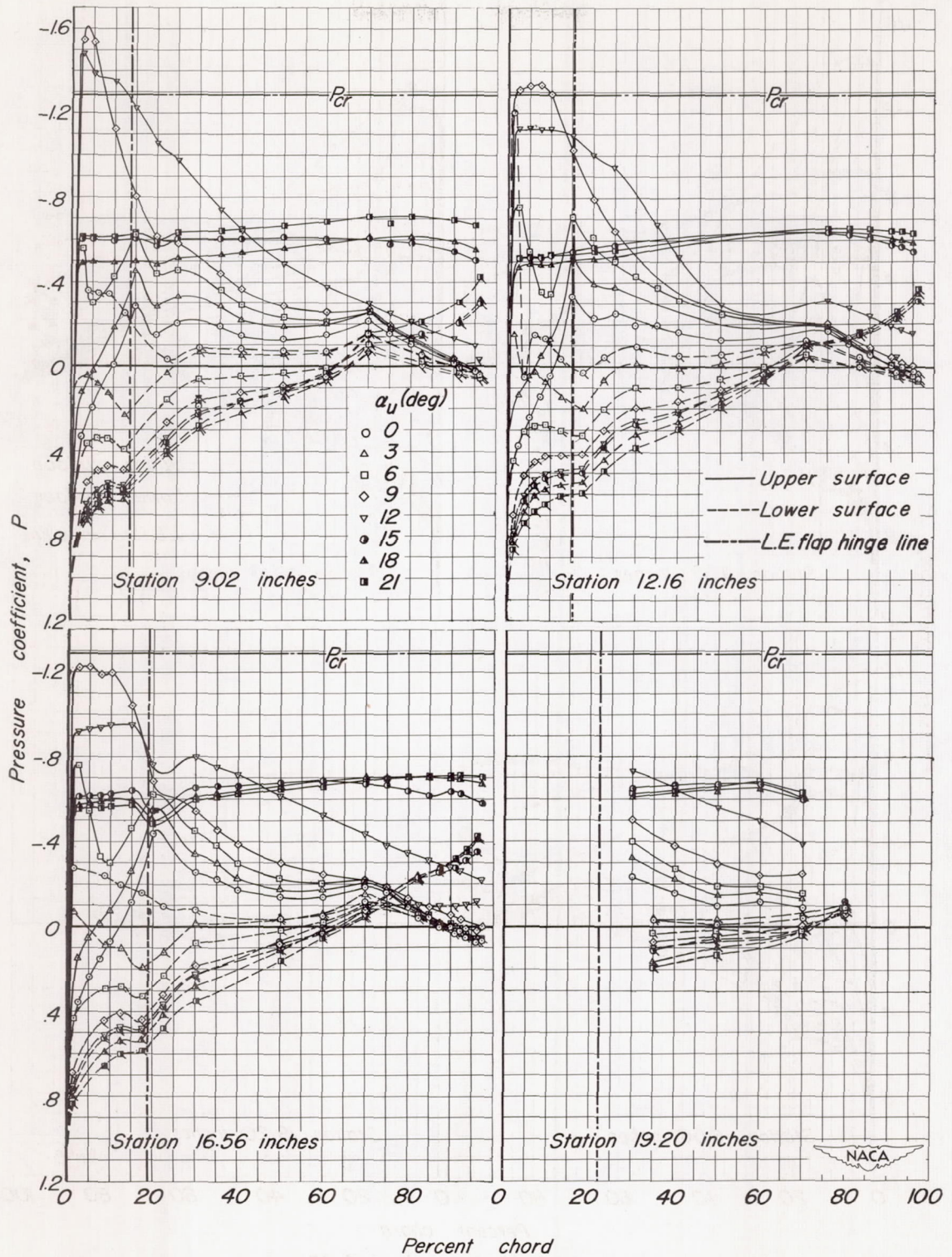
(e) Mach number, 0.925.

Figure 5.—Concluded.



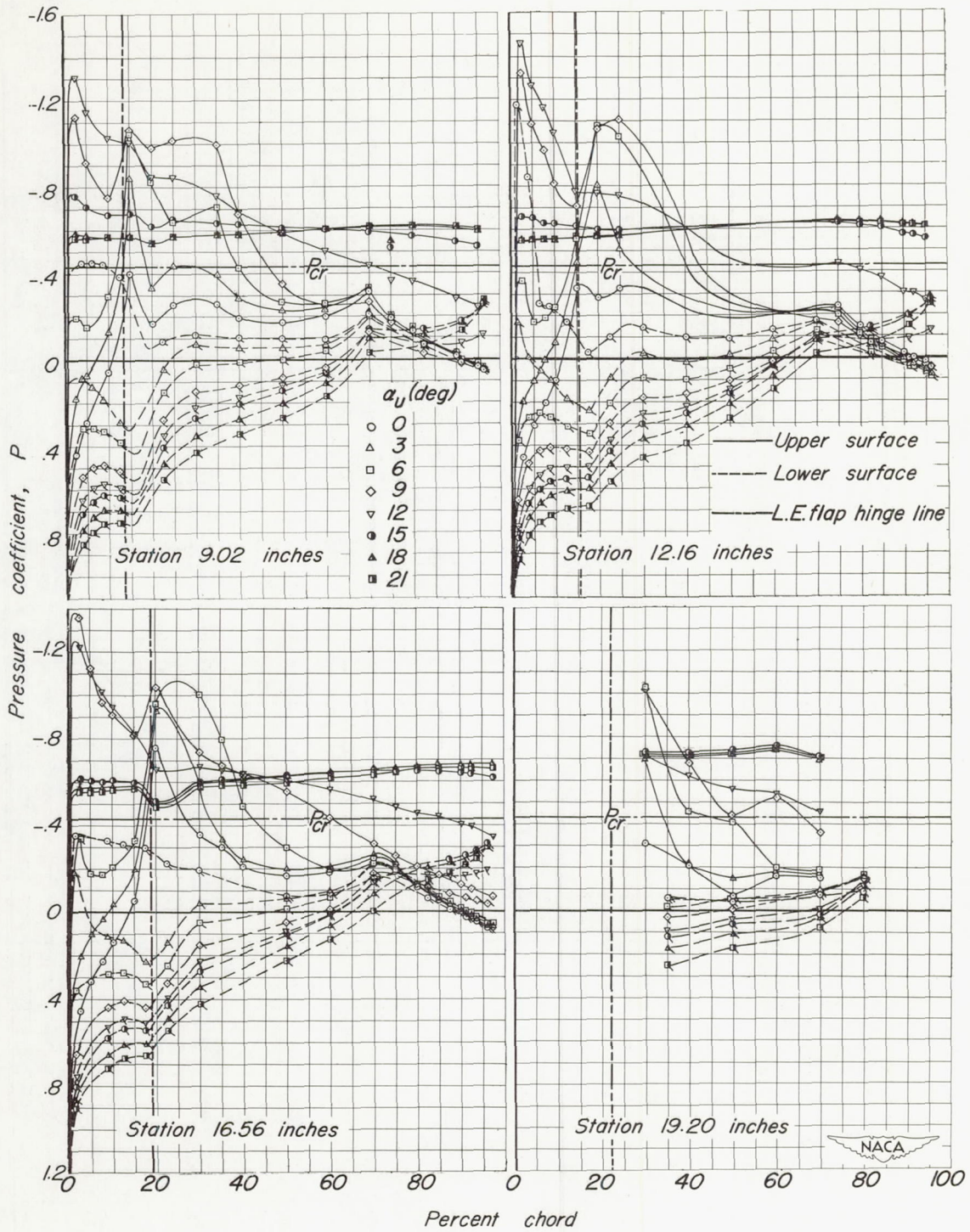
(a) Mach number, 0.40.

Figure 6.- The pressure distribution over the wing of the X-3 model.  $\psi_v, 0^\circ$ ;  $\delta_{lf}, 10^\circ$



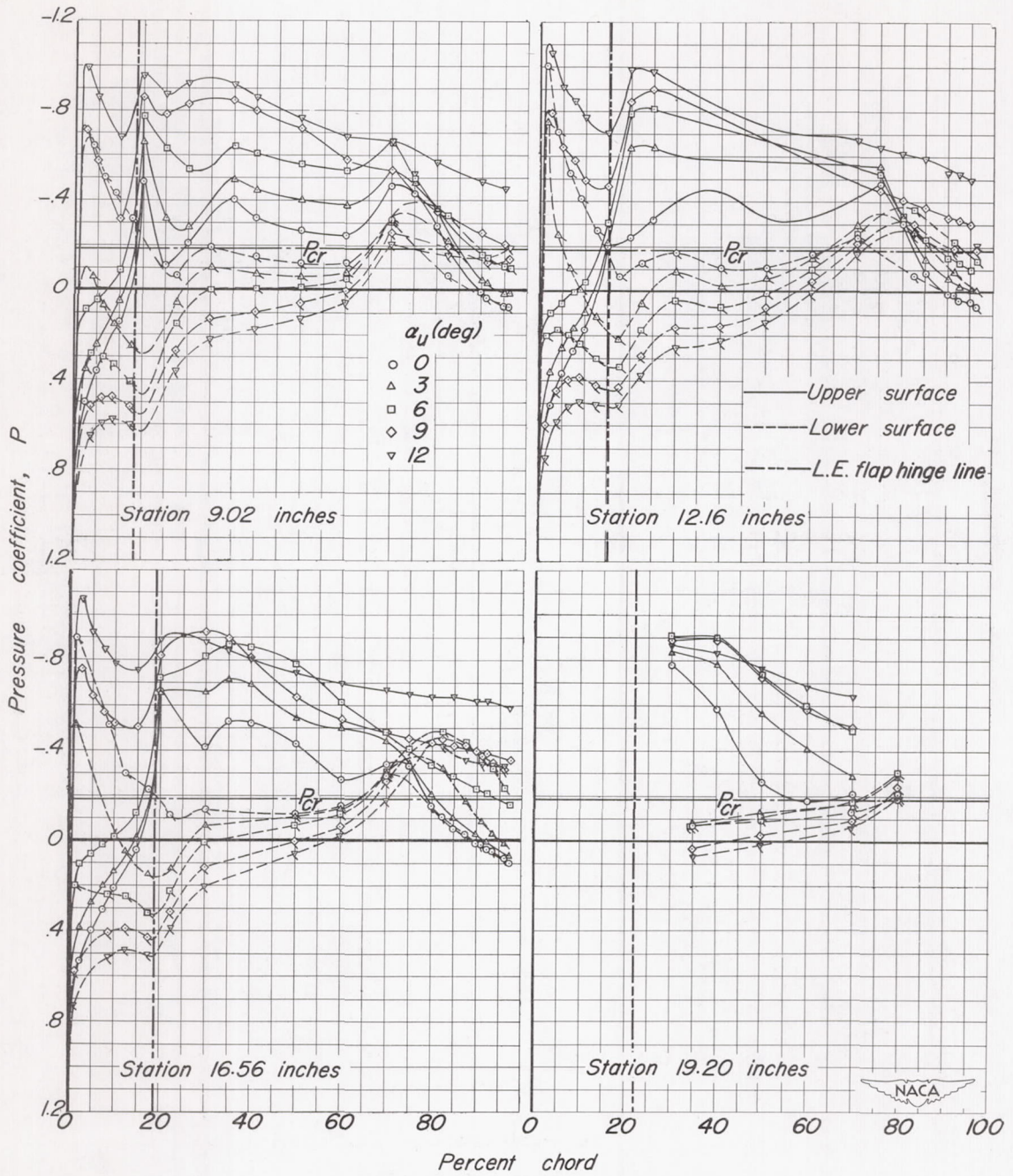
(b) Mach number, 0.60.

Figure 6.—Continued.



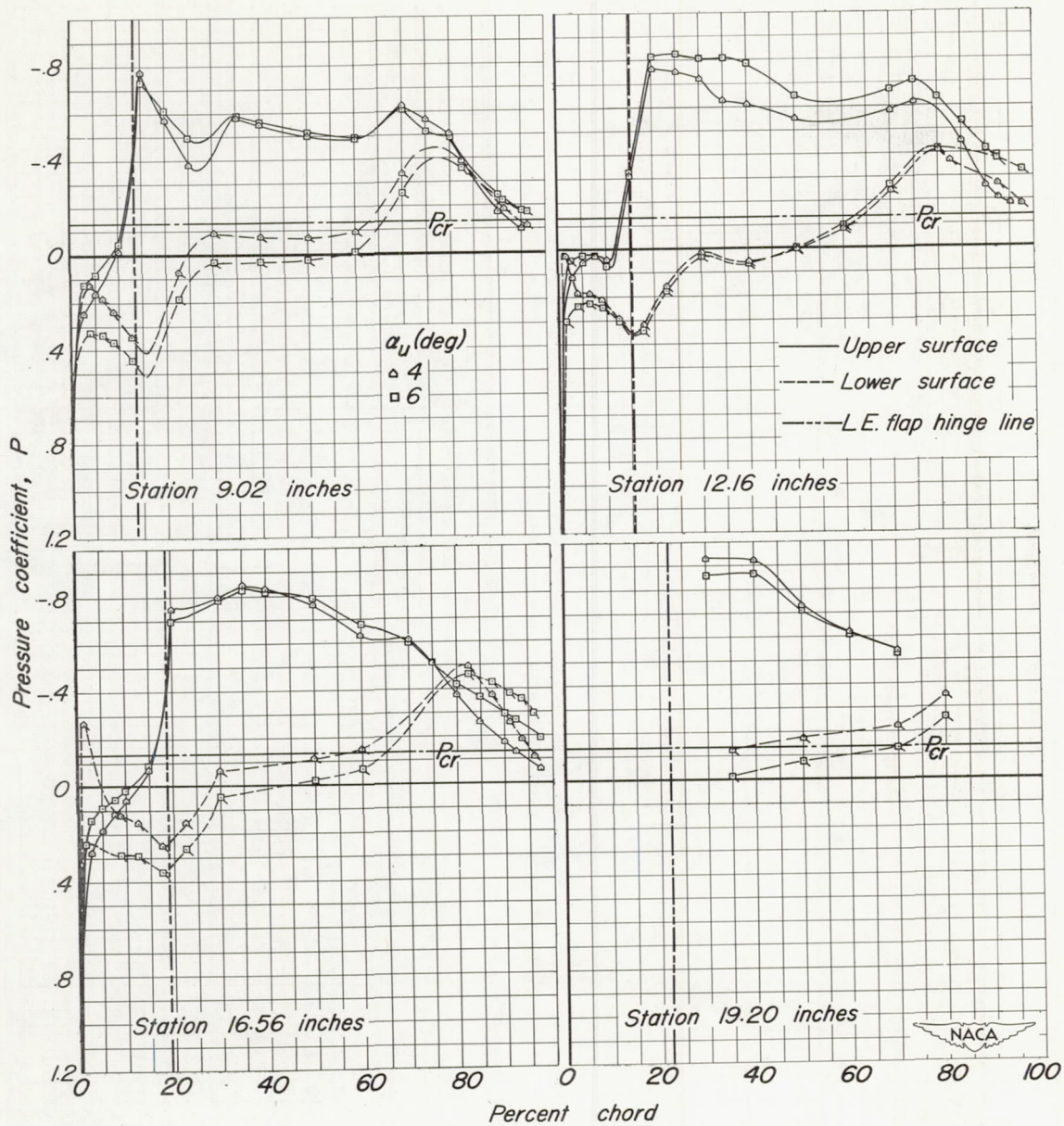
(c) Mach number 0.80.

Figure 6.-Continued.



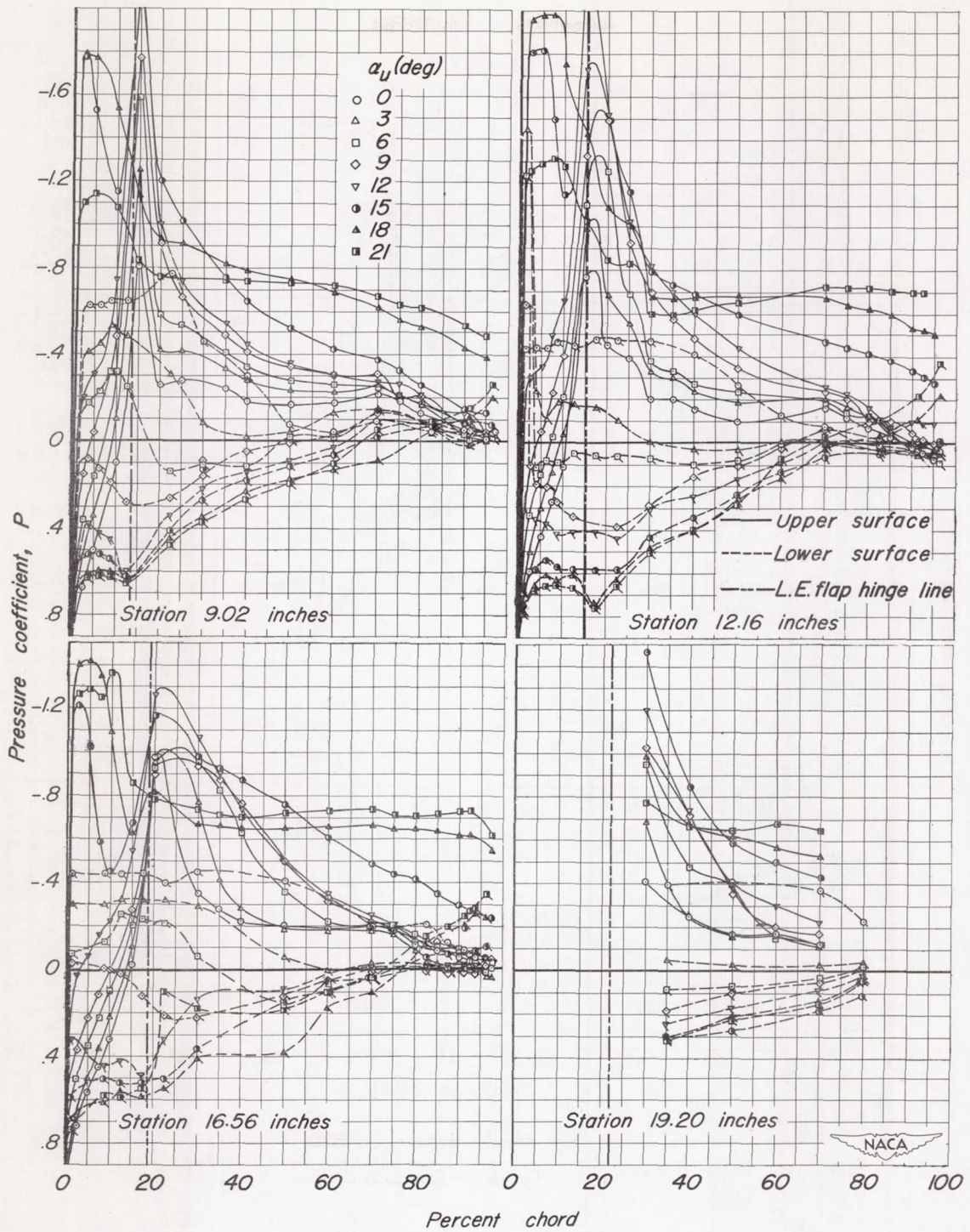
(d) Mach number, 0.90.

Figure 6.-Continued.



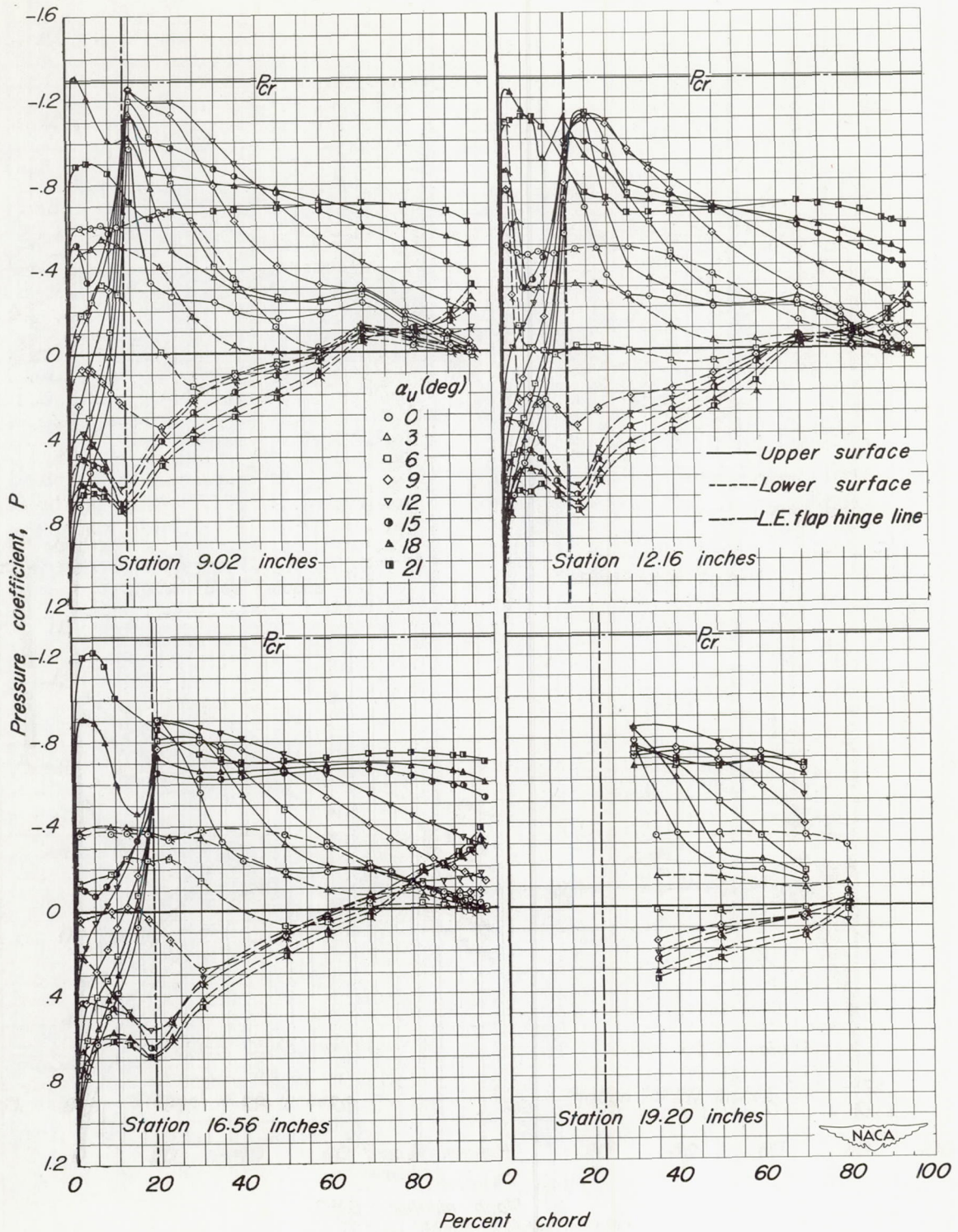
(e) Mach number, 0.925.

Figure 6—Concluded.



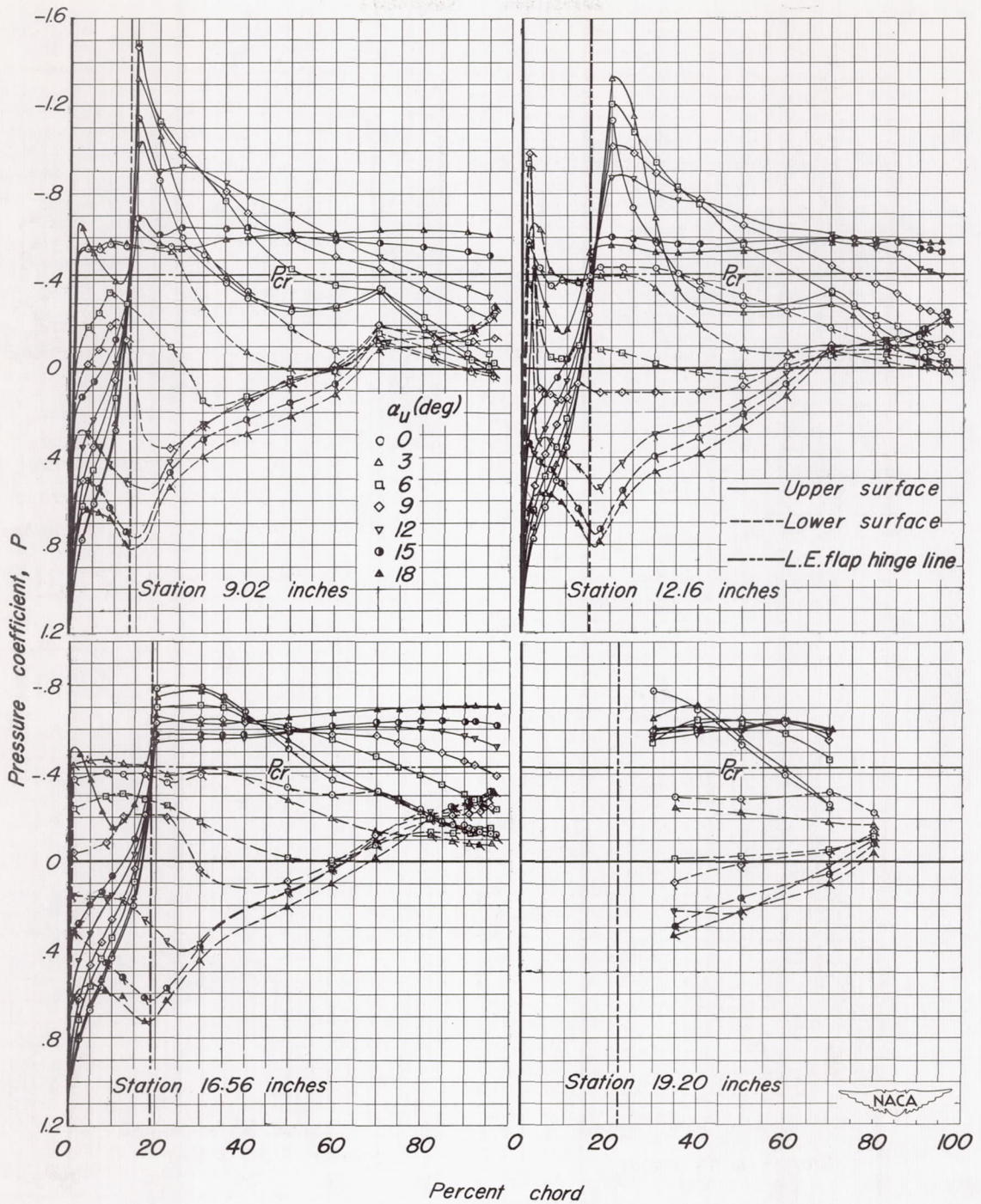
(a) Mach number, 0.40.

Figure 7.- The pressure distribution over the wing of the X-3 model.  $\psi_u, 0^\circ$ ;  $\delta_{lf}, 30^\circ$ .



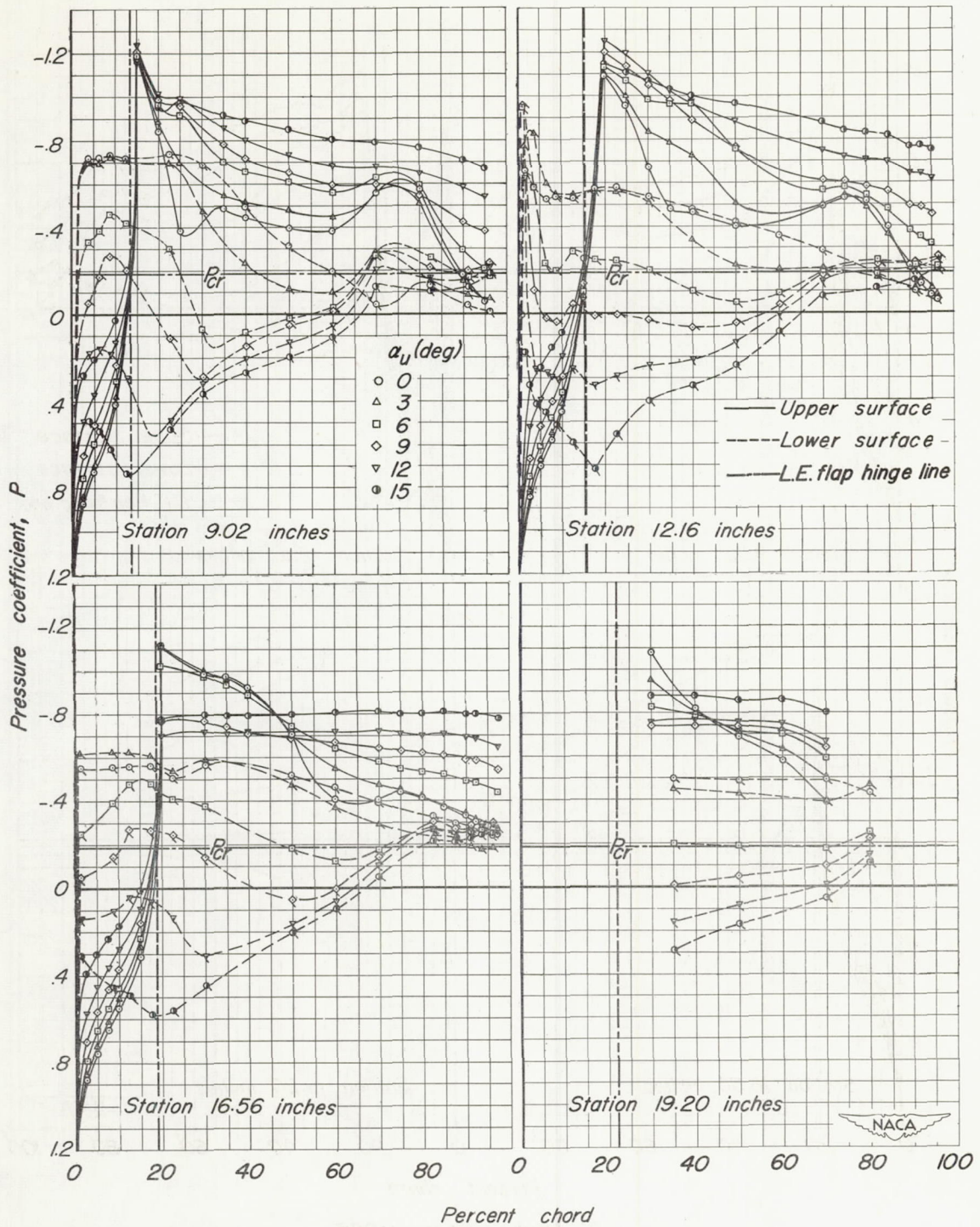
(b) Mach number, 0.60.

Figure 7-Continued.



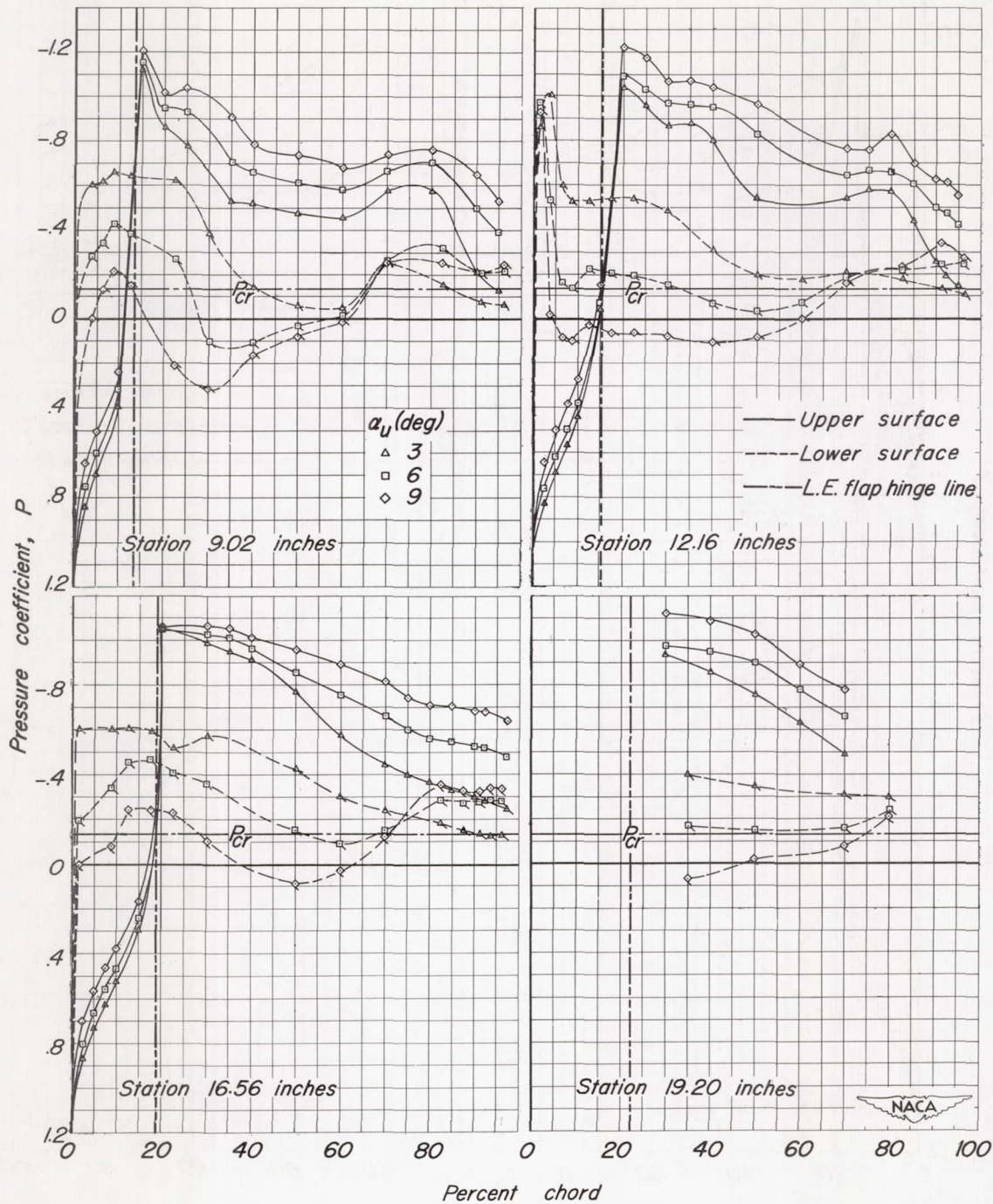
(c) Mach number 0.80.

Figure 7—Continued.



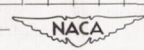
(d) Mach number, 0.90.

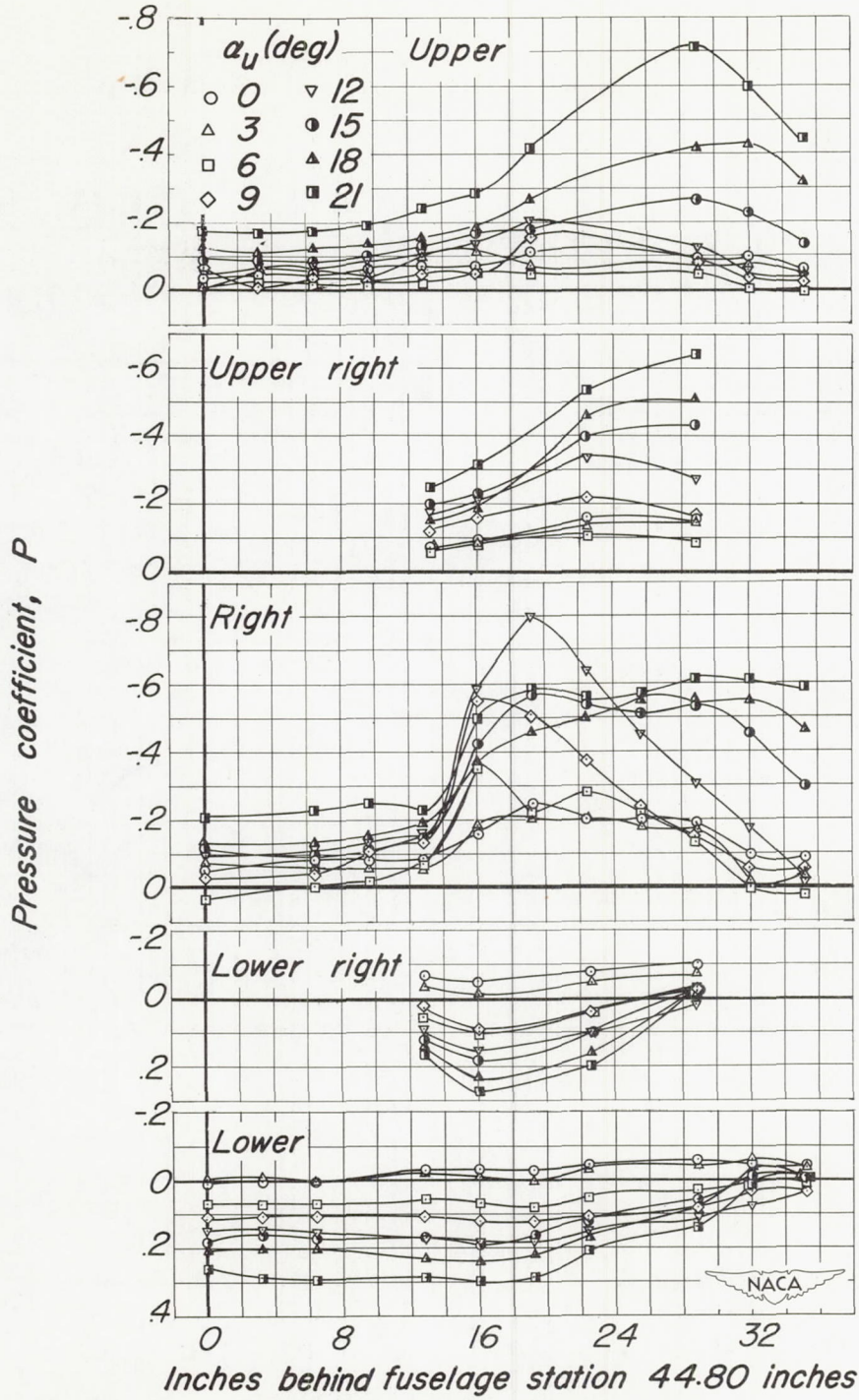
Figure 7.—Continued.



(e) Mach number, 0.925

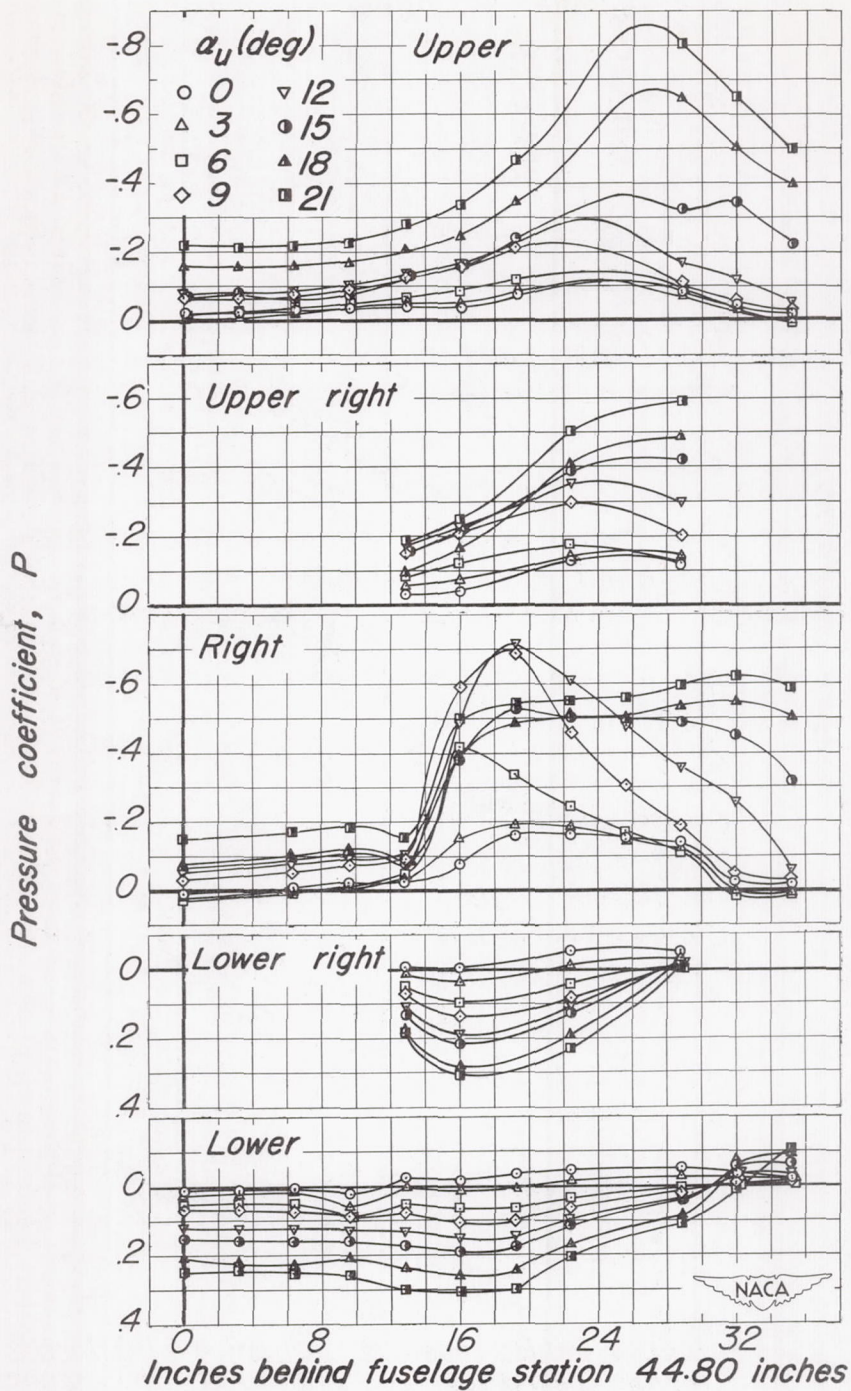
Figure 7.—Concluded.





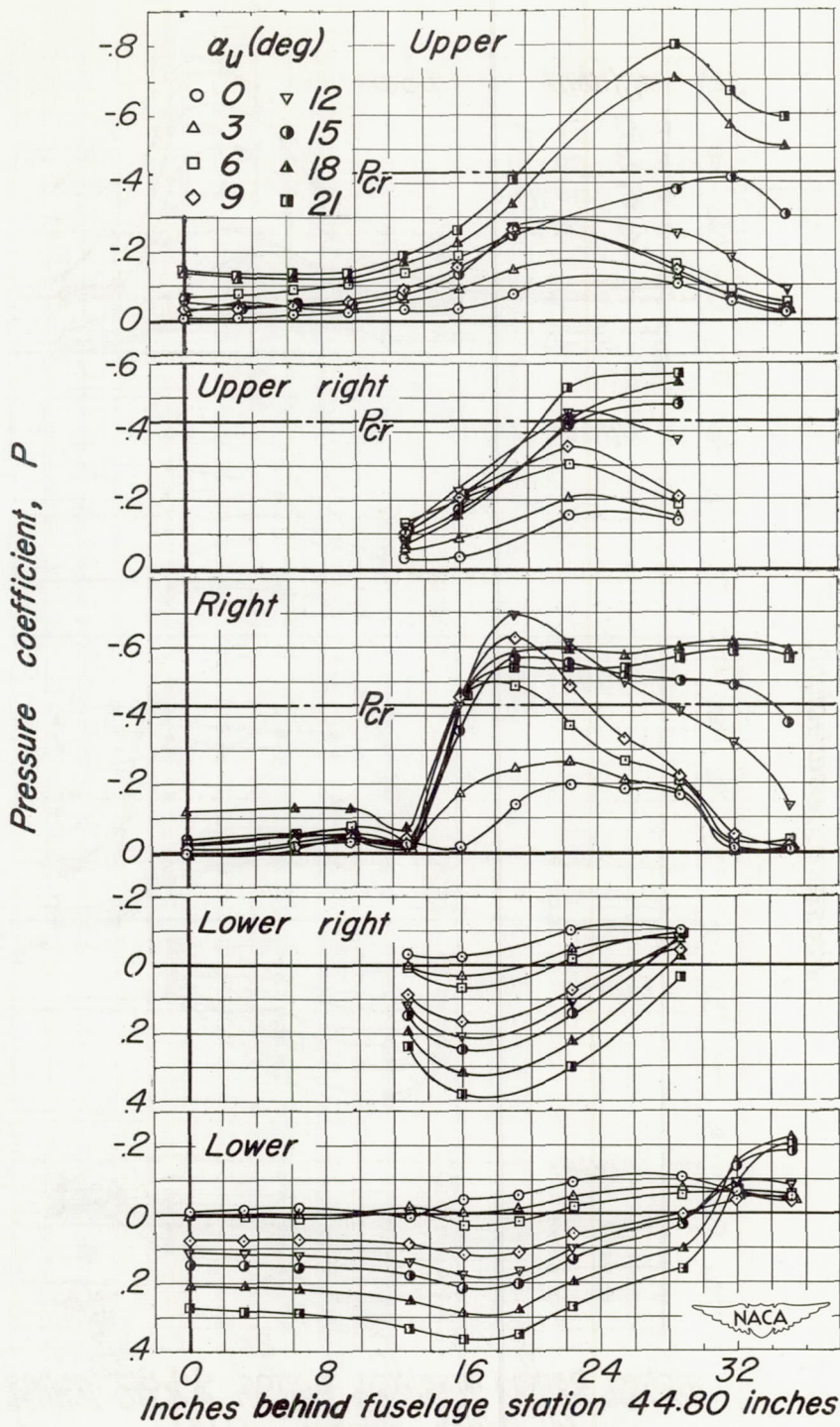
(a) Mach number, 0.40.

Figure 8.-The pressure distribution over the fuselage of the X-3 model.  $\psi_U, 0^\circ; \delta_{lf}, 0^\circ$



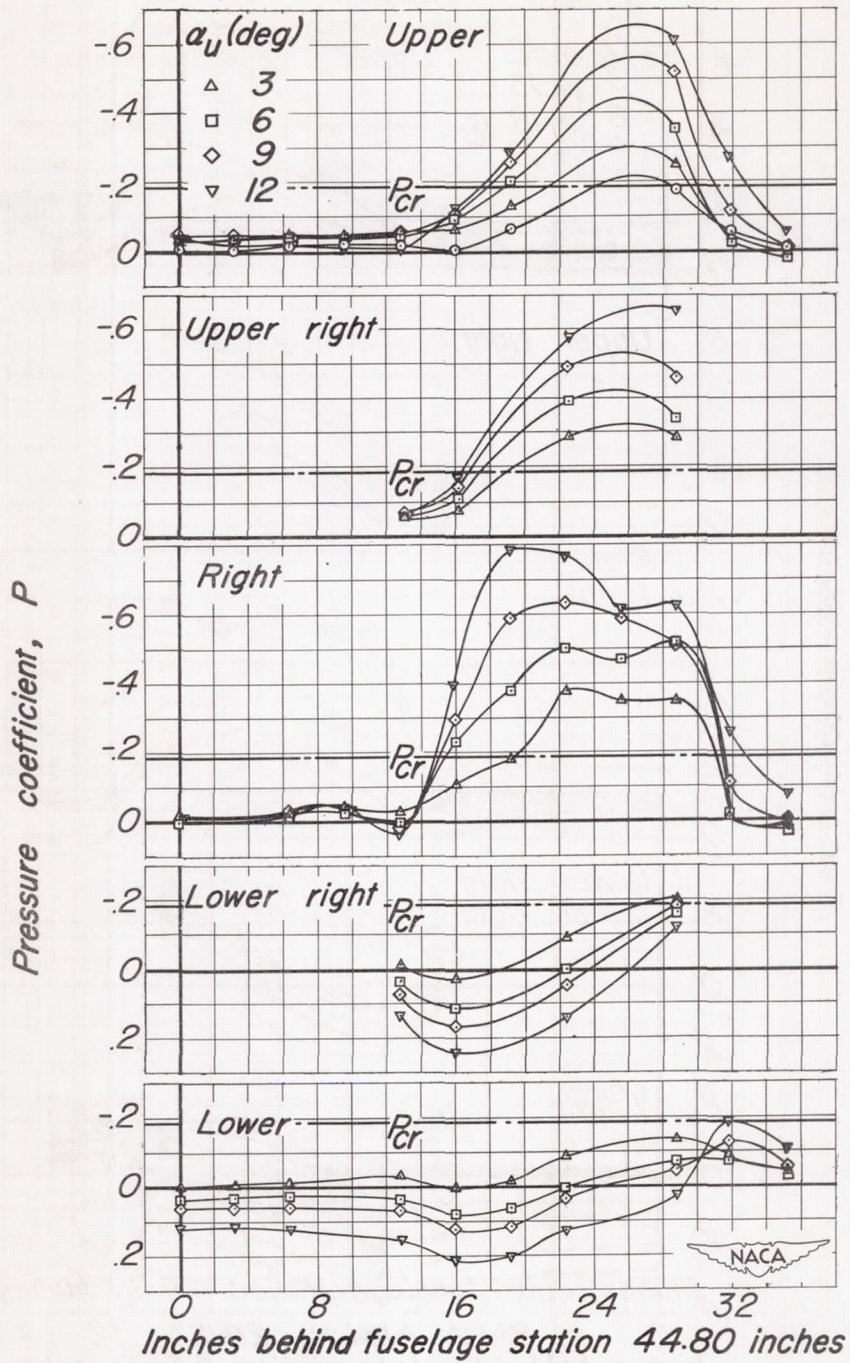
(b) Mach number, 0.60.

Figure 8.-Continued.



(c) Mach number 0.80.

Figure 8.-Continued.



(d) Mach number, 0.90.

Figure 8.—Continued.

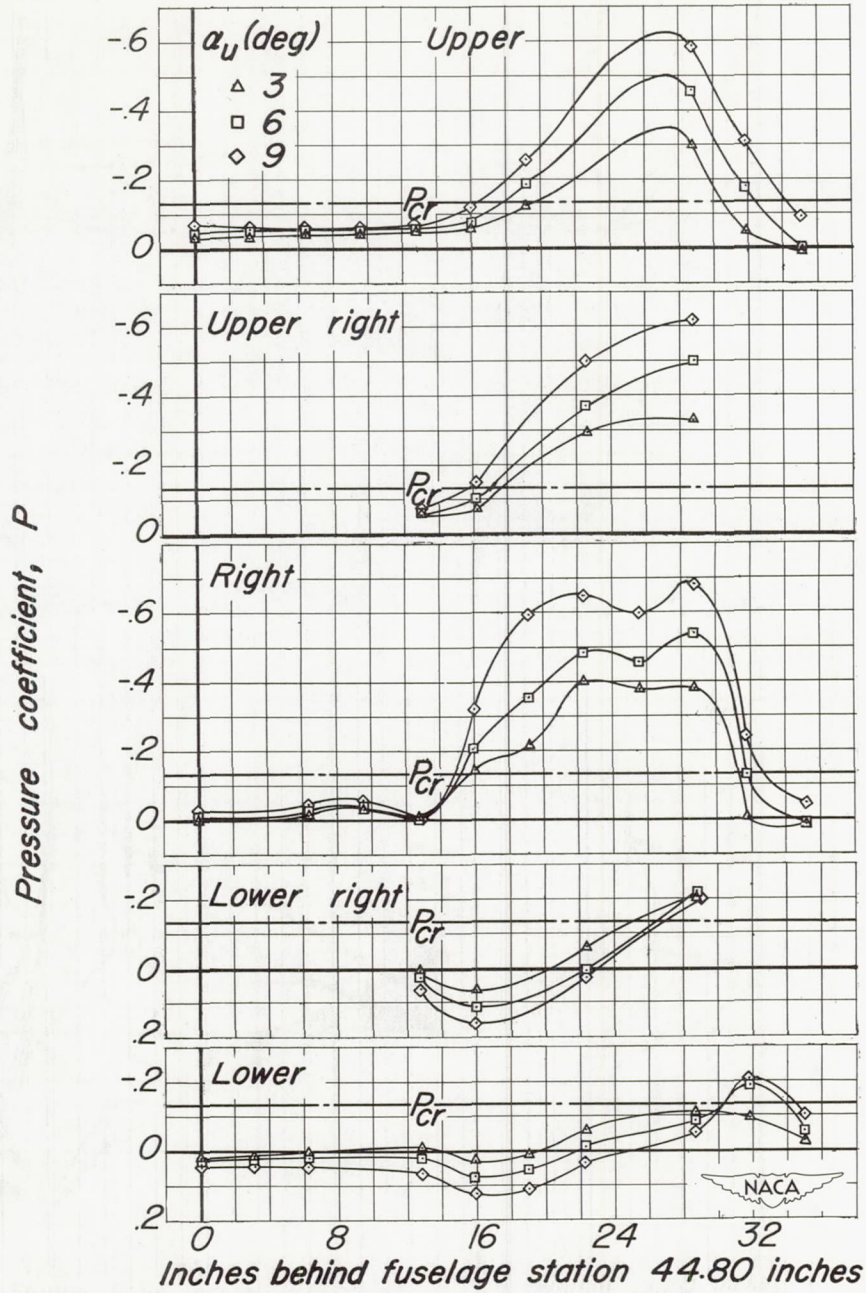


Figure 8.-Concluded.

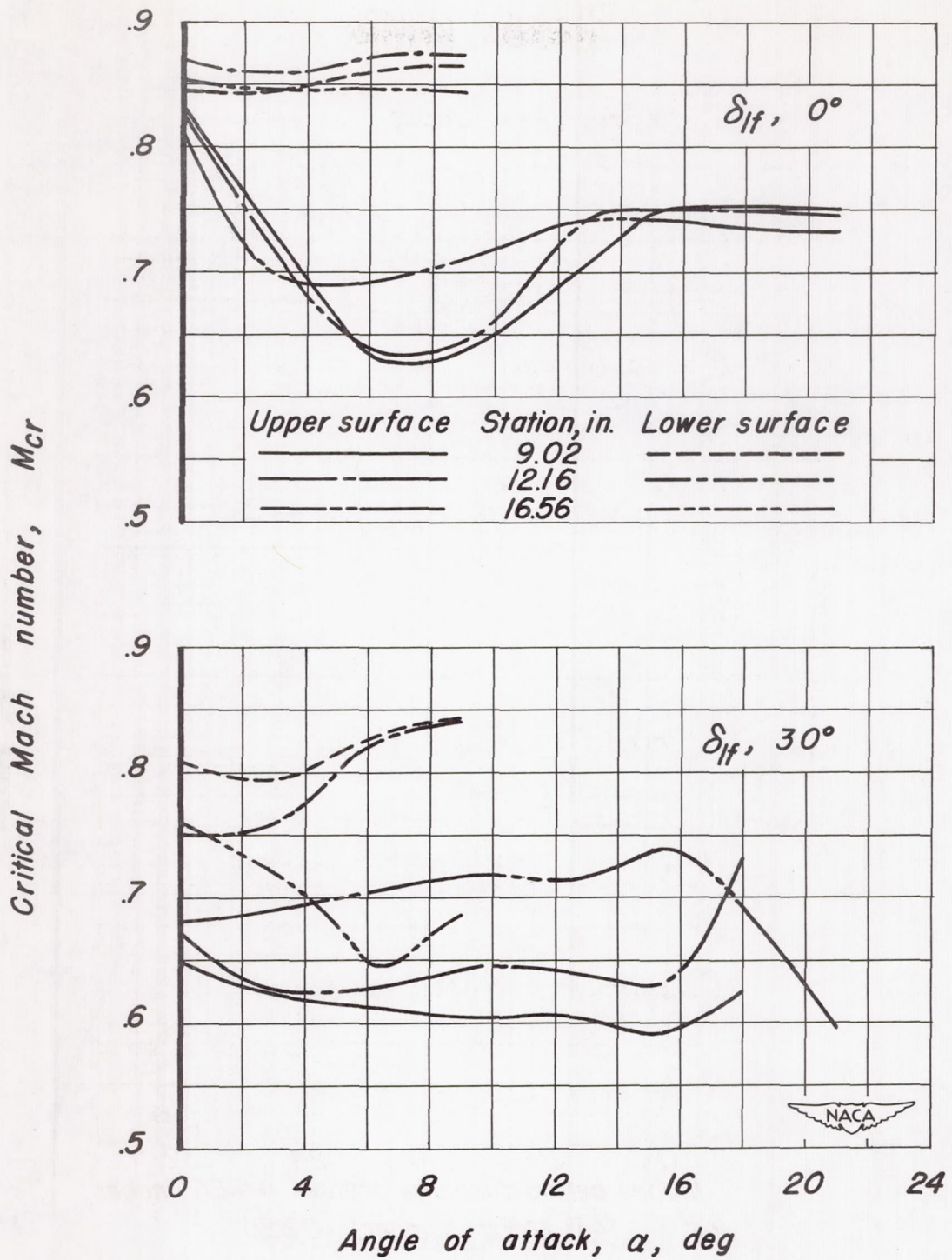


Figure 9.—The critical Mach number characteristics of the wing of the X-3 model.  $\psi_u, 0^\circ$

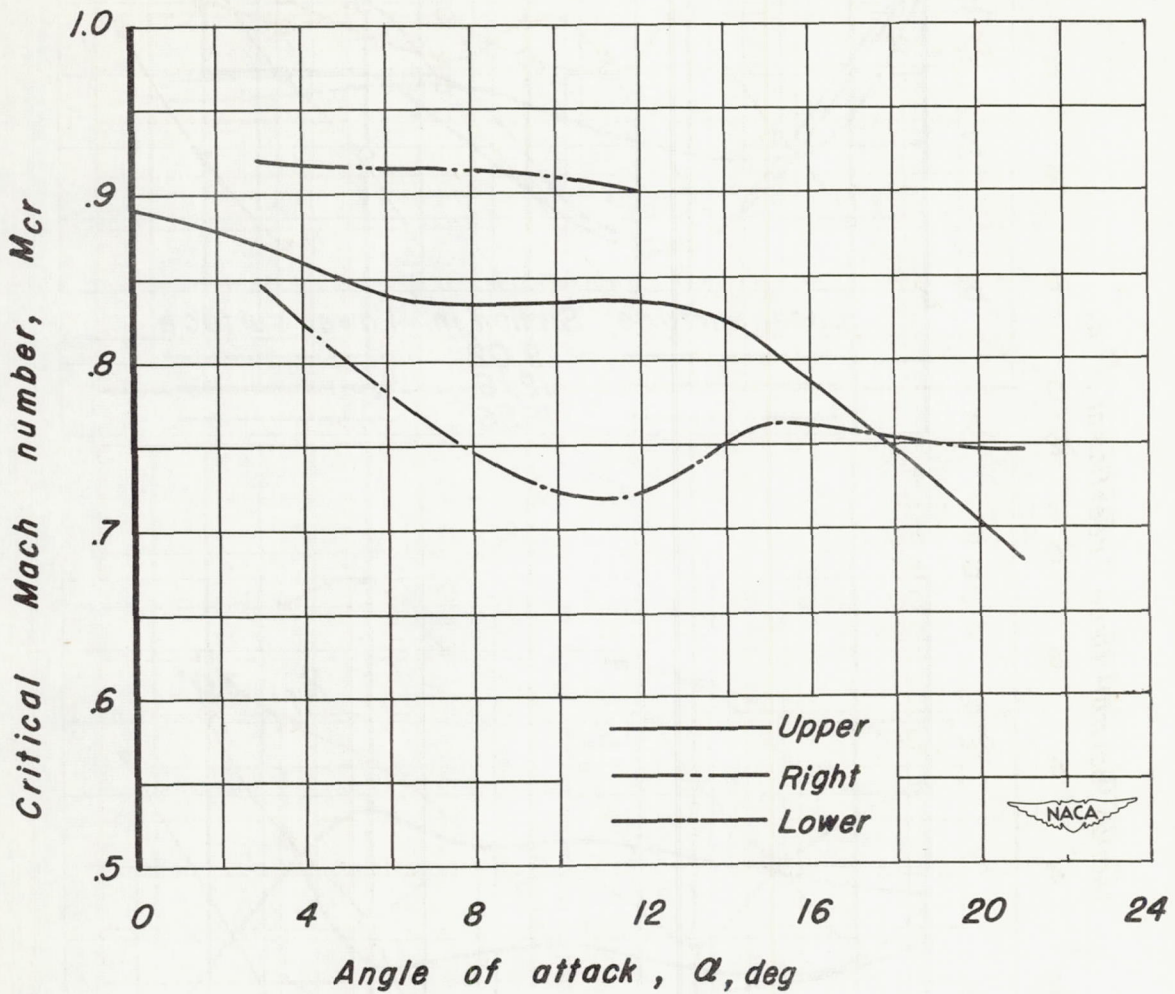
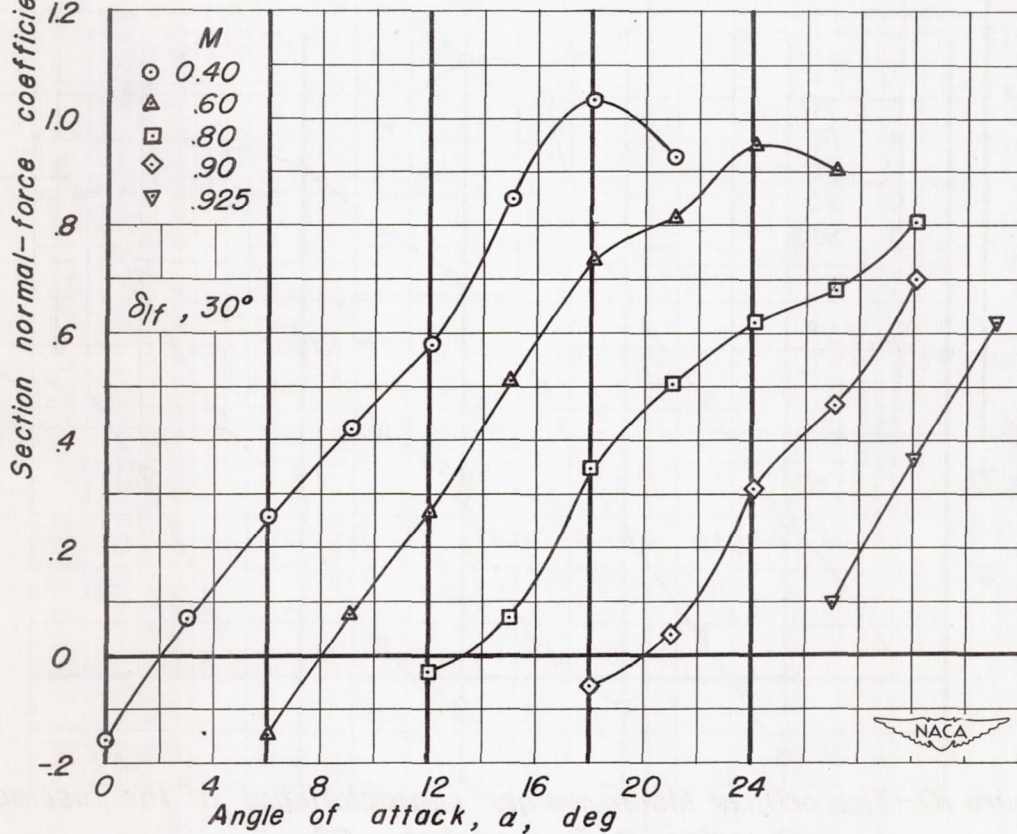
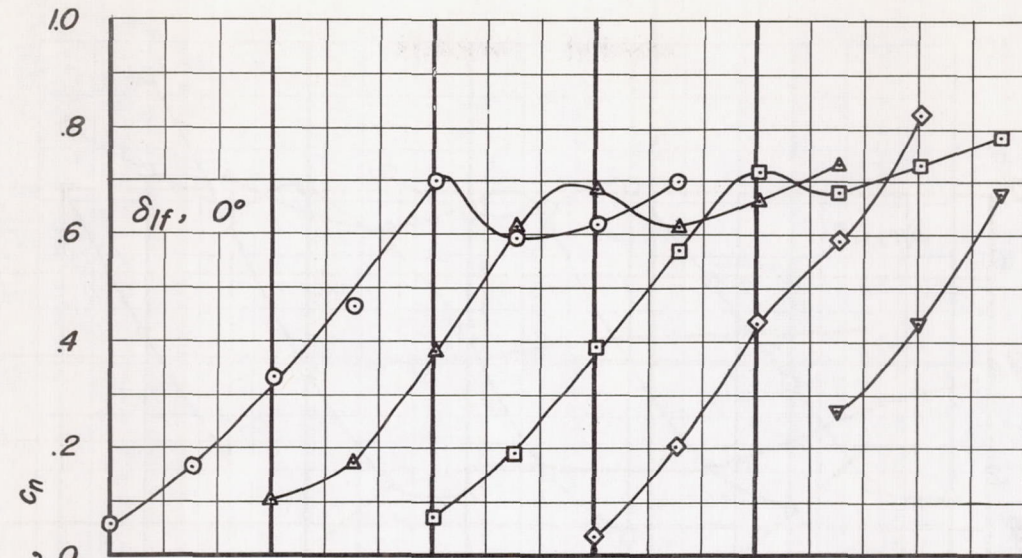


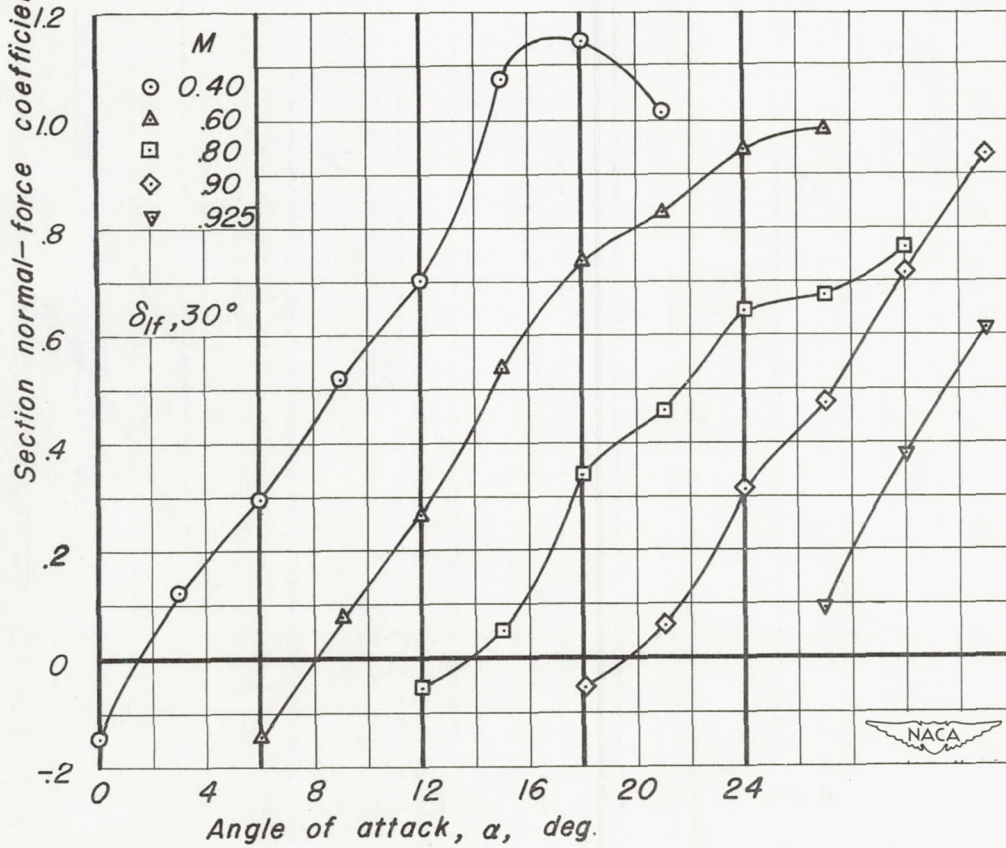
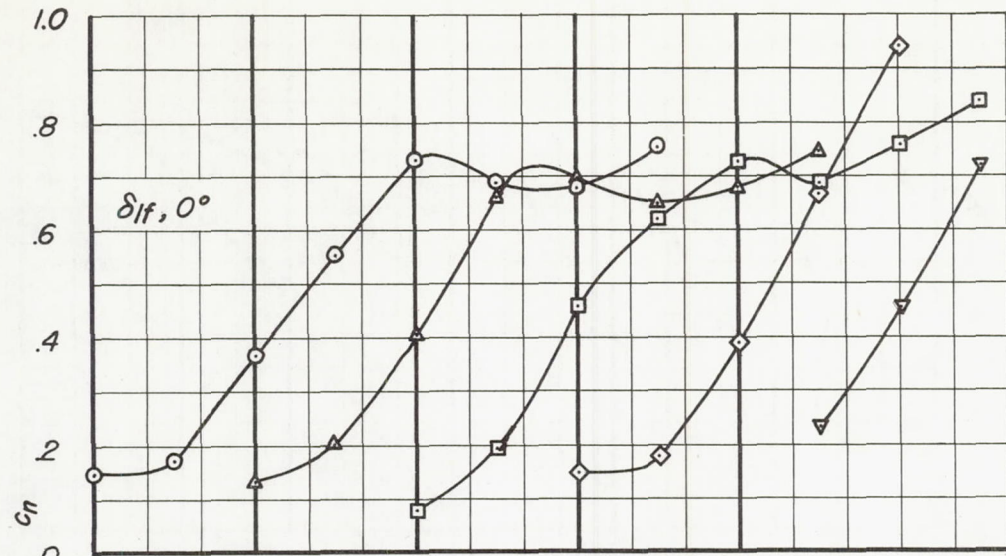
Figure 10.-The critical Mach number characteristics of the fuselage of the X-3 model.  $\psi_u, 0^\circ$



$\alpha$ of 0 for	0	0	0	0
M of 4	.6	.8	.9	.925

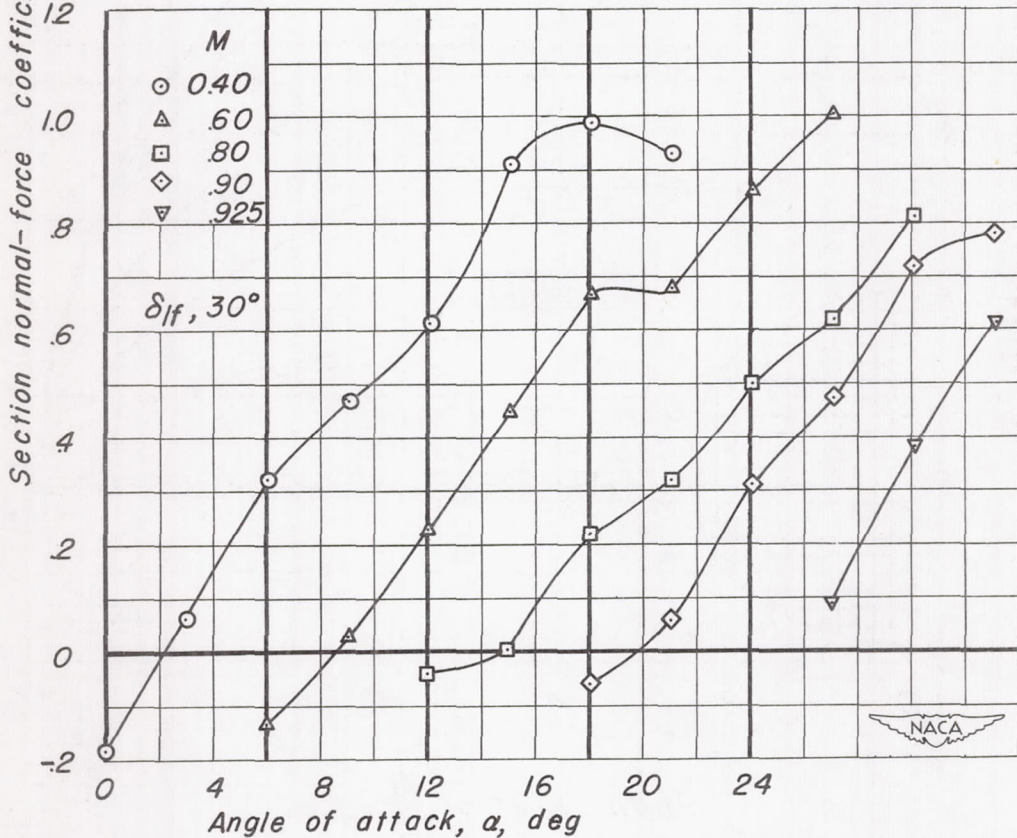
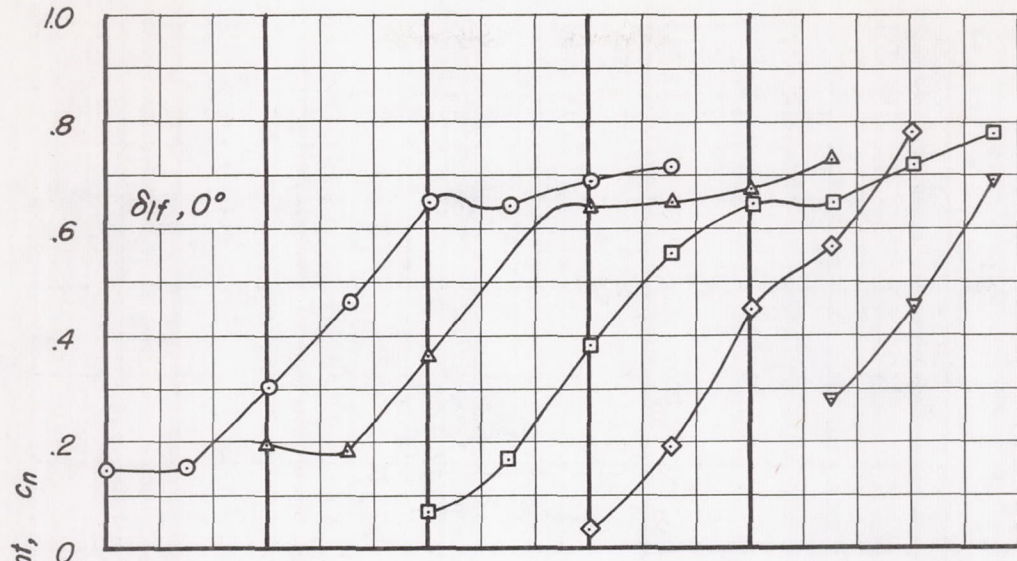
(a) Wing station 9.02 inches

Figure 11.-The section normal-force characteristics of the wing of the X-3 model.  $\psi_w, 0^\circ$



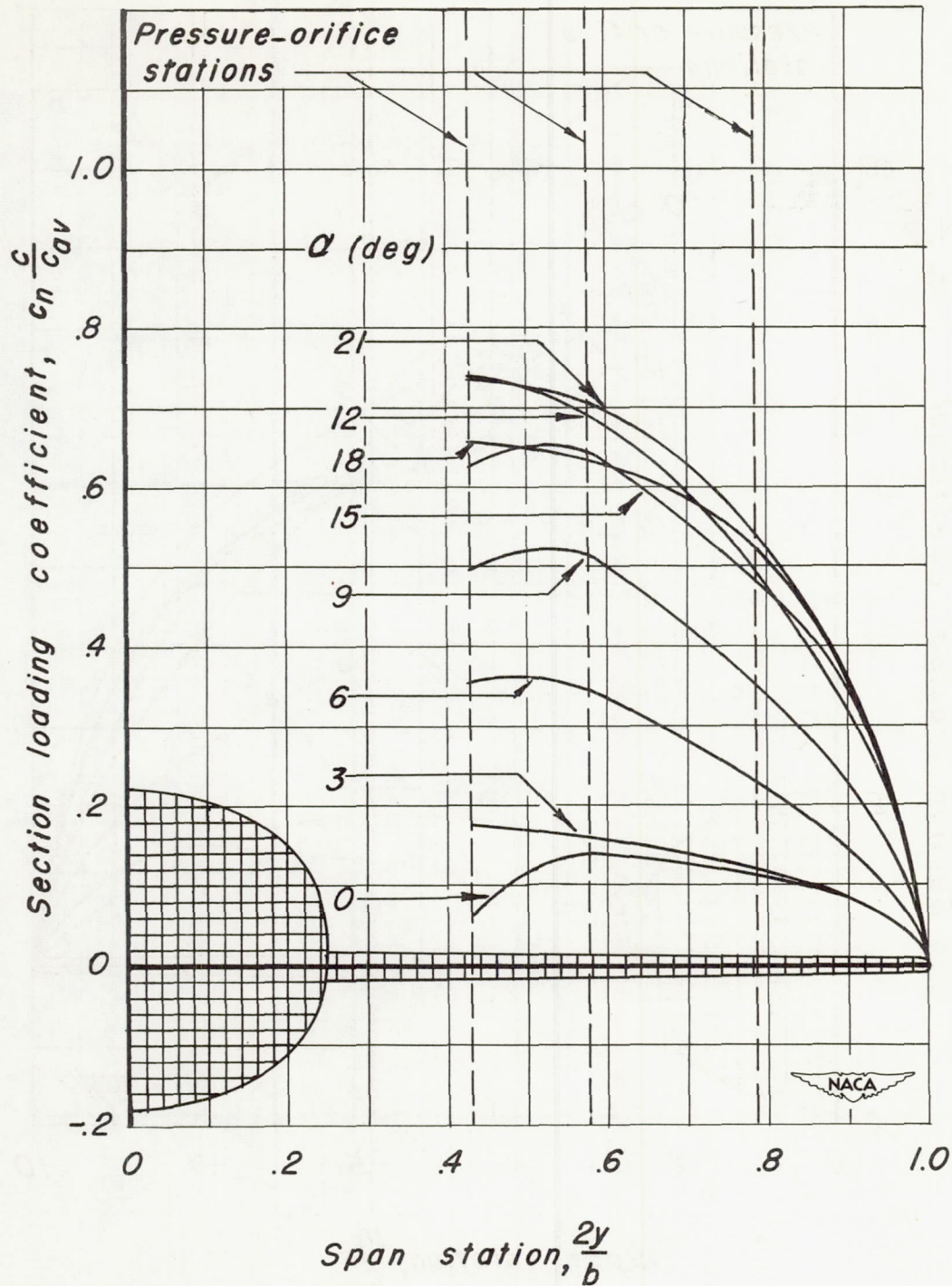
$\alpha$ of 0 for	0	0	0	0
$M$ of .4	.6	.8	.9	.925

(b) Wing station 12.16 inches.  
Figure 11.-Continued.



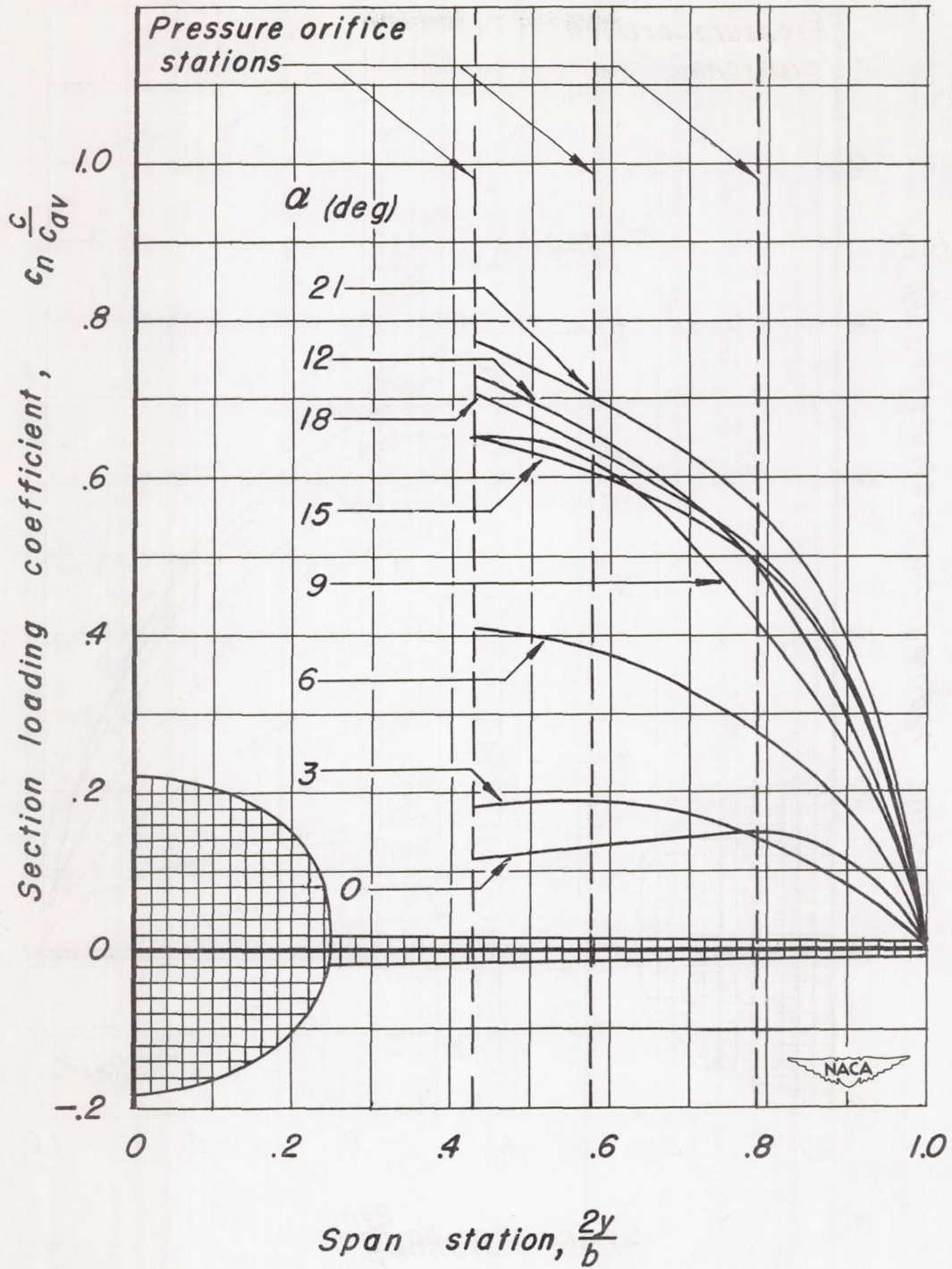
$\alpha$ of 0 for	0	0	0	0
$M$ of 4	.6	.8	.9	.925

(c) Wing station 16.56 inches.  
Figure 11.- Concluded.

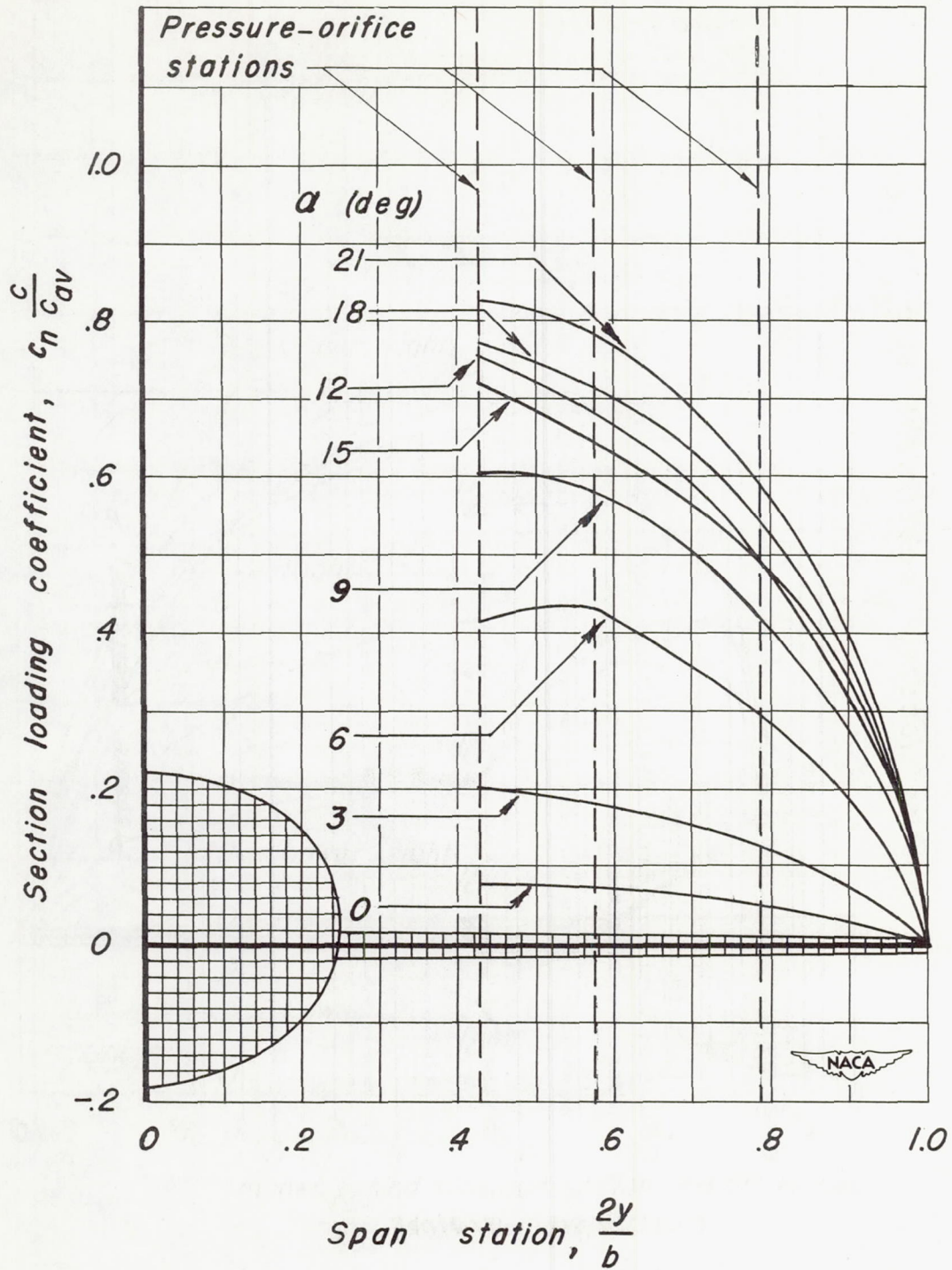


(a) Mach number, 0.40.

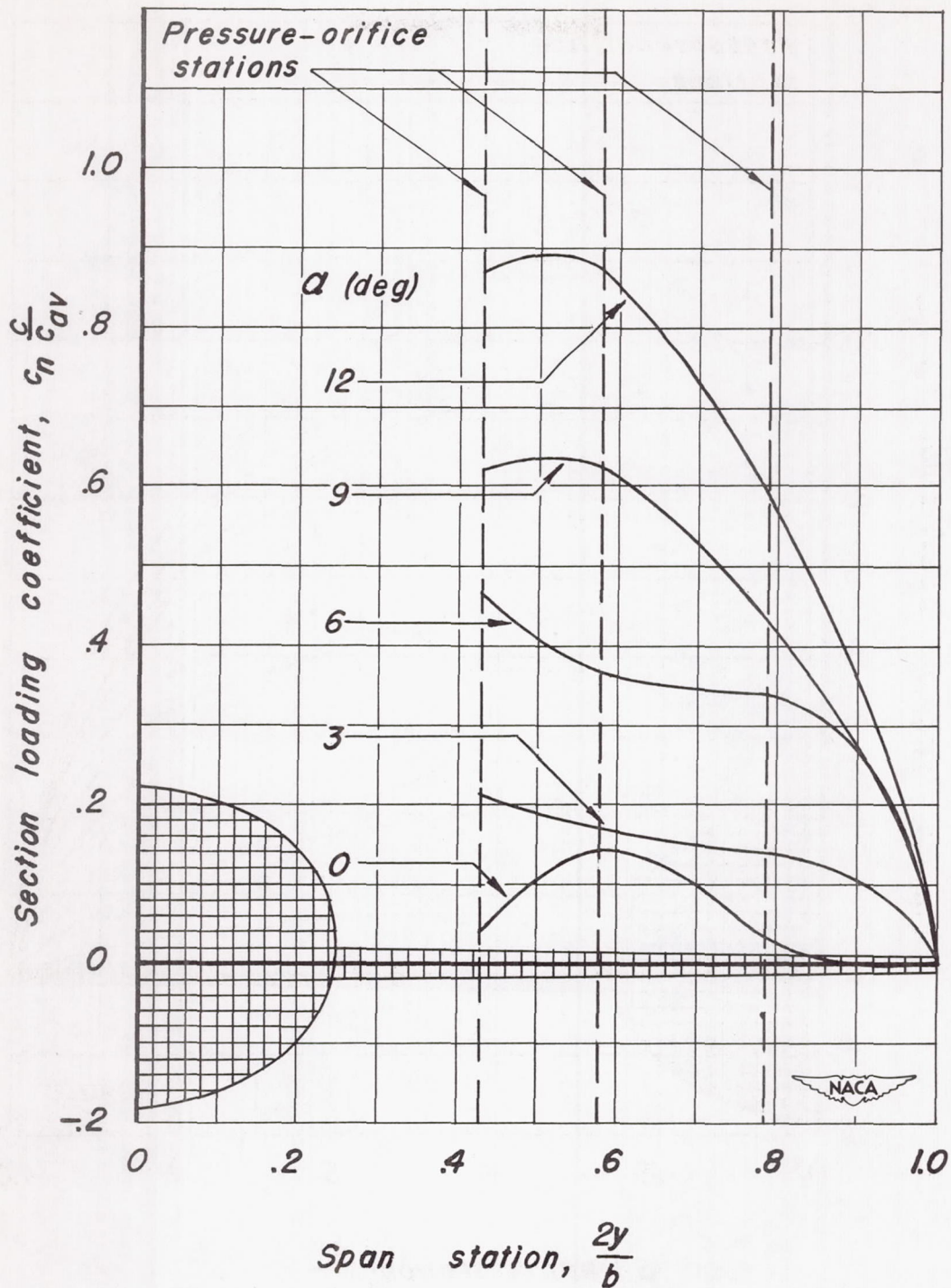
Figure 12.—The spanwise distribution of load on the wing of the X-3 model.  $\psi_u, 0^\circ$ ;  $\delta_{lf}, 0^\circ$



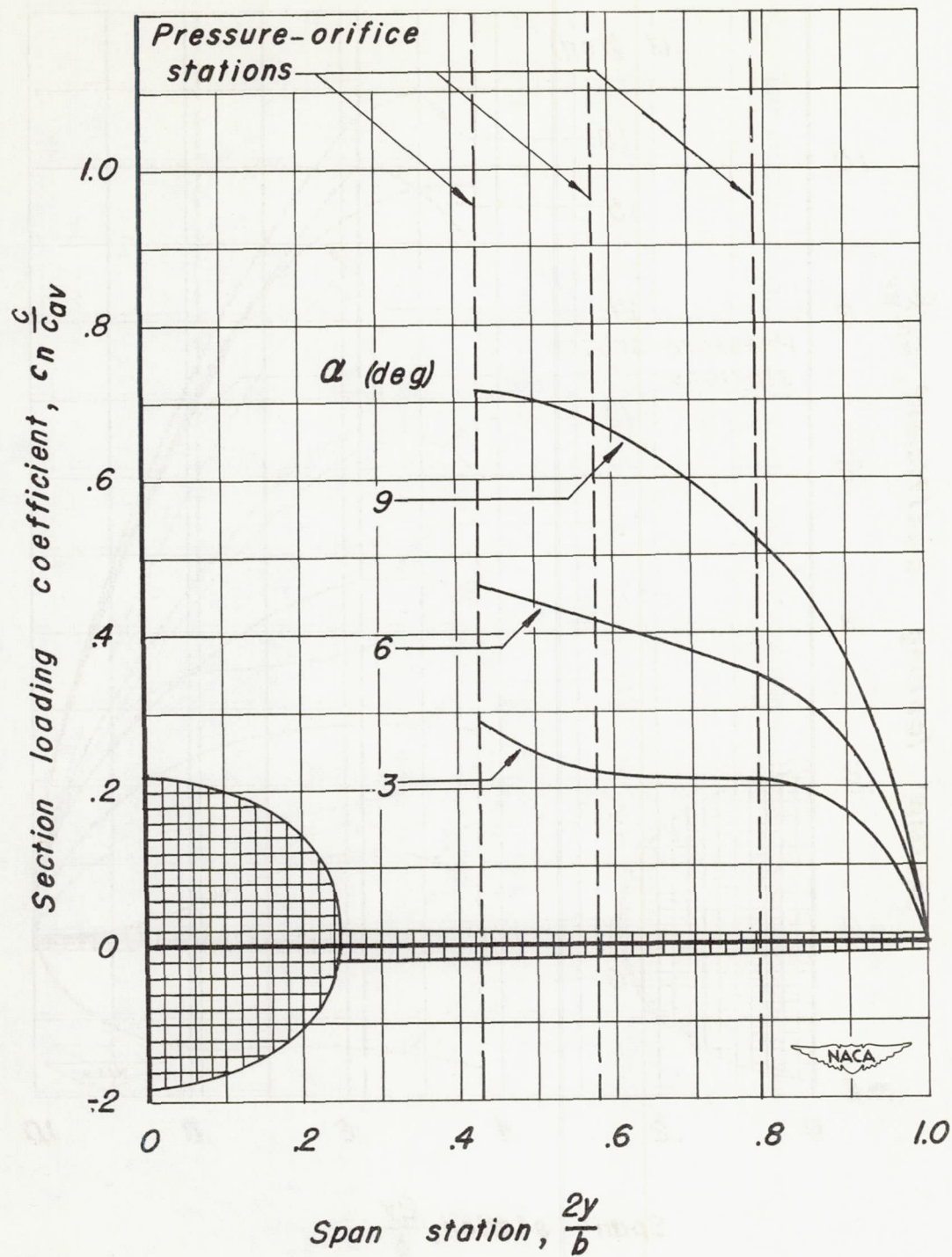
(b) Mach number, 0.60.  
Figure 12.-Continued.



(c) Mach number, 0.80.  
Figure 12.—Continued.

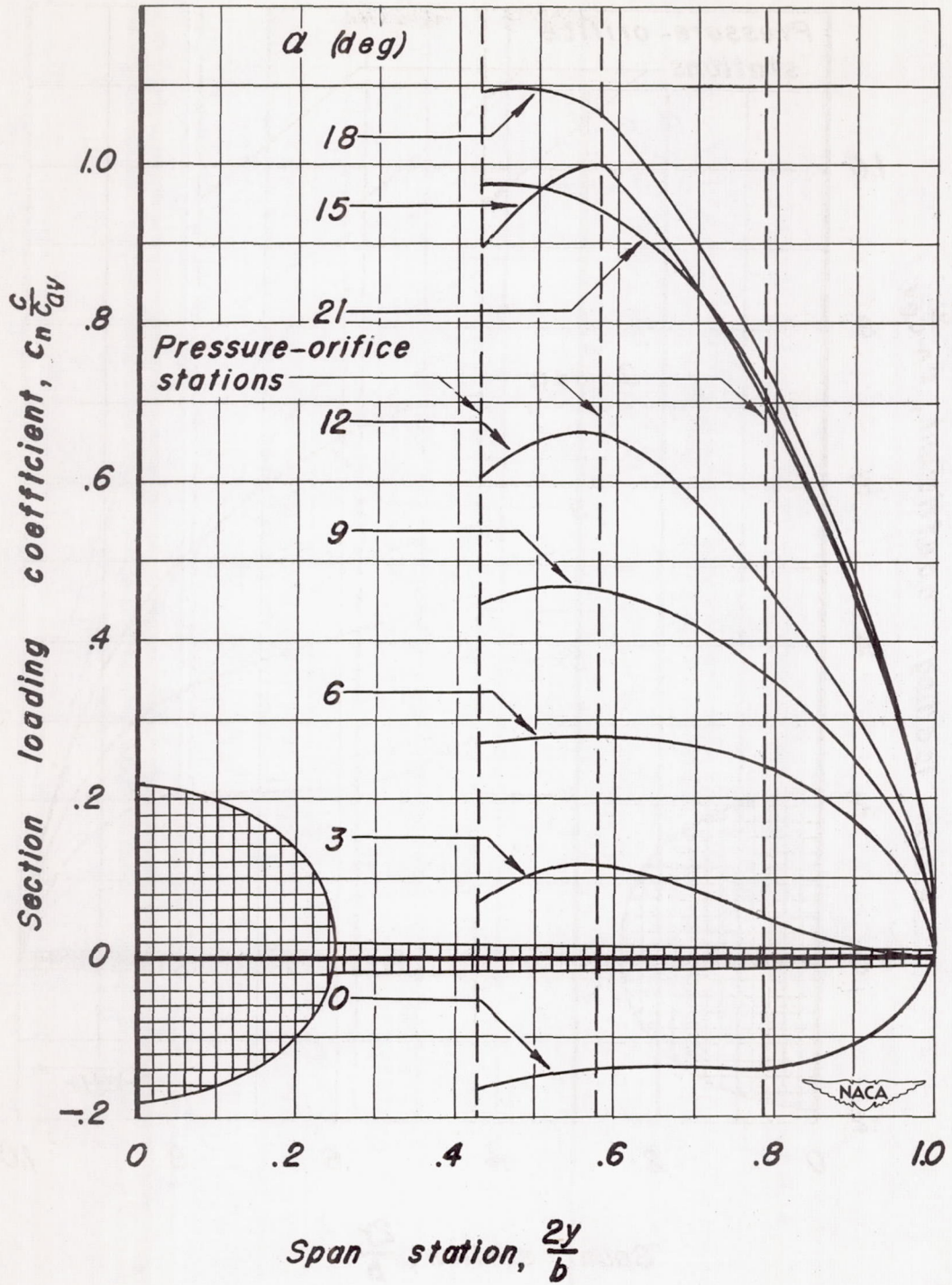


(d) Mach number, 0.90.  
Figure 12.-Continued.



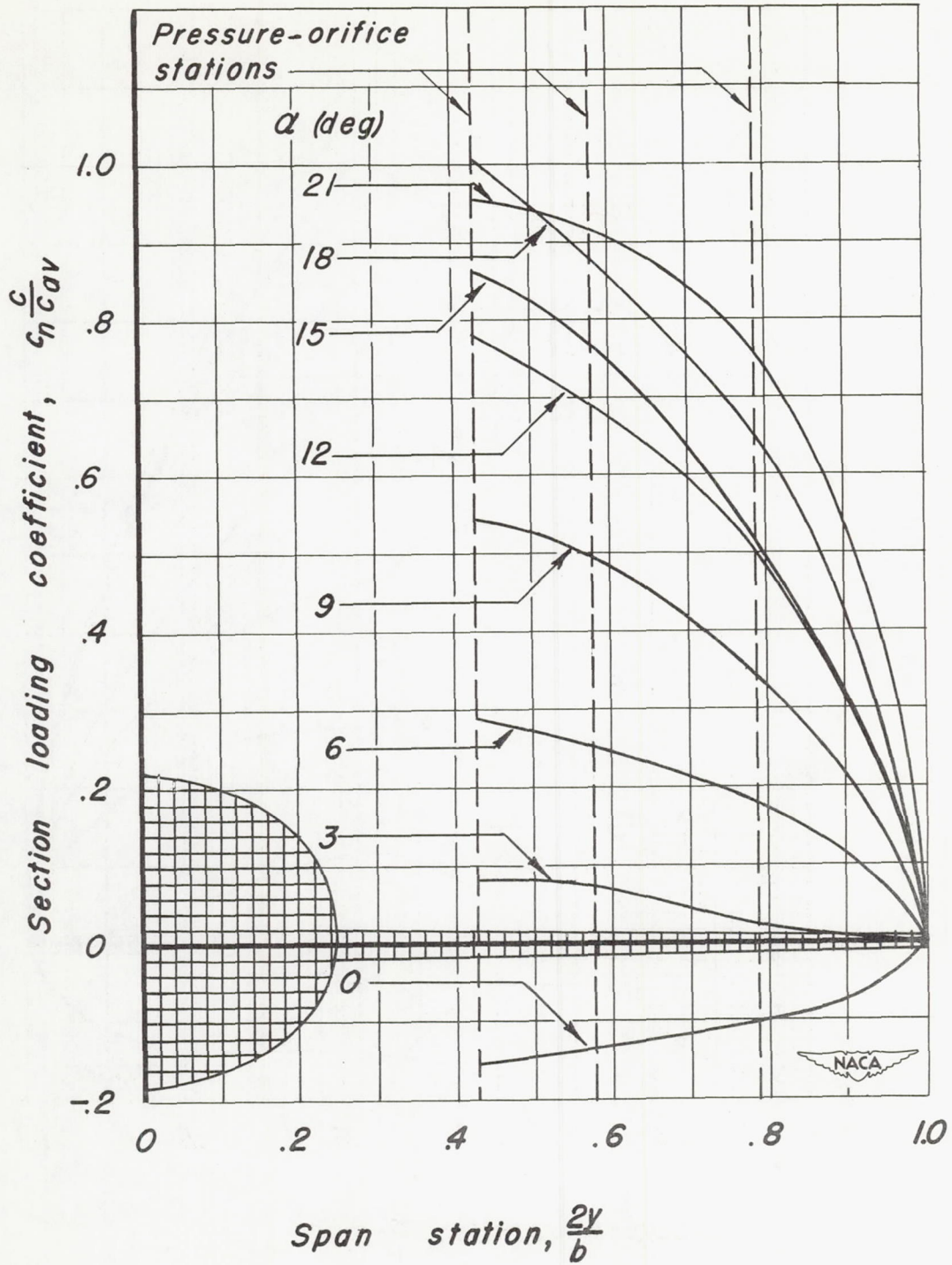
(e) Mach number, 0.925.

Figure 12.-Concluded.

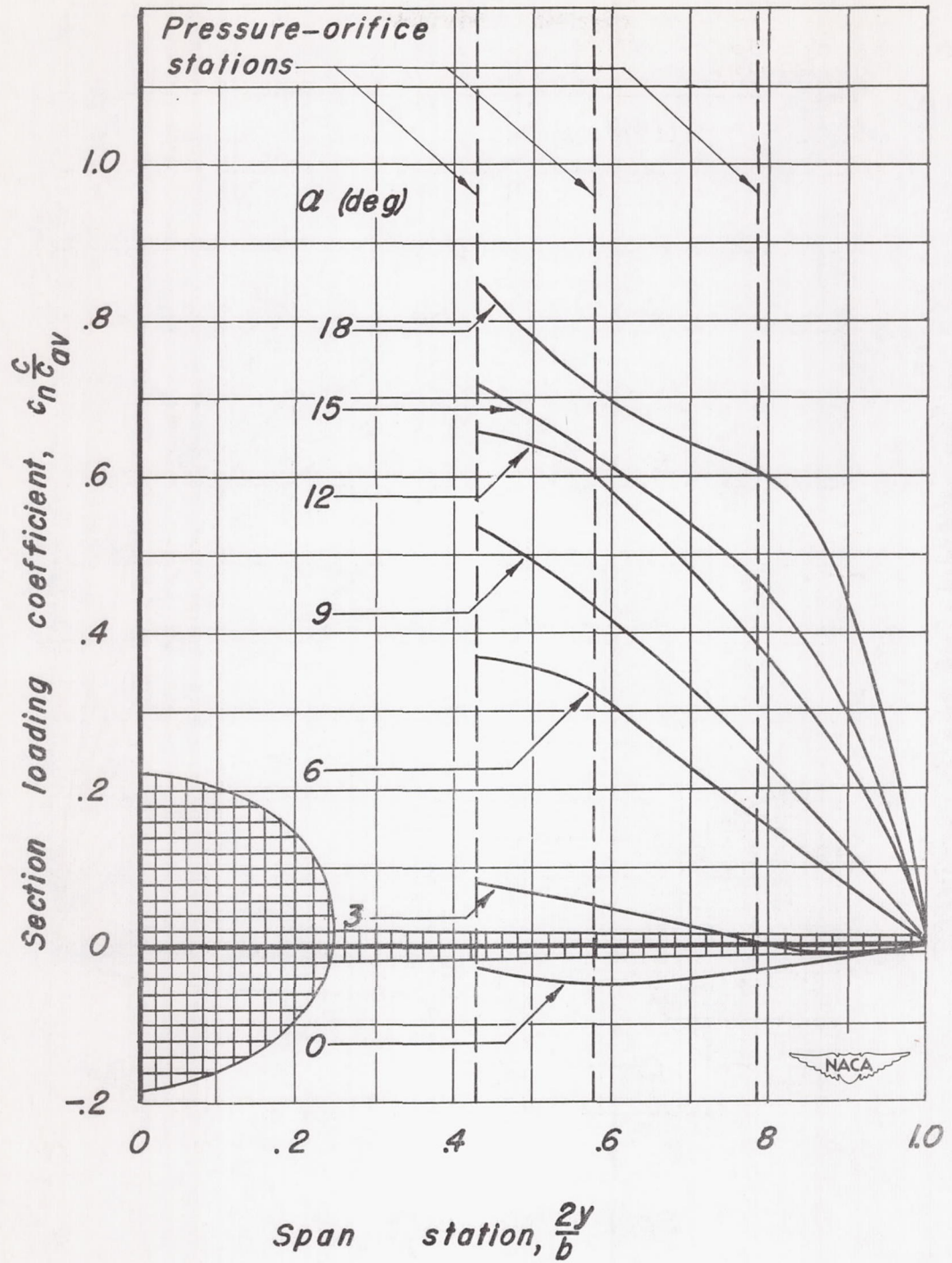


(a) Mach number, 0.40.

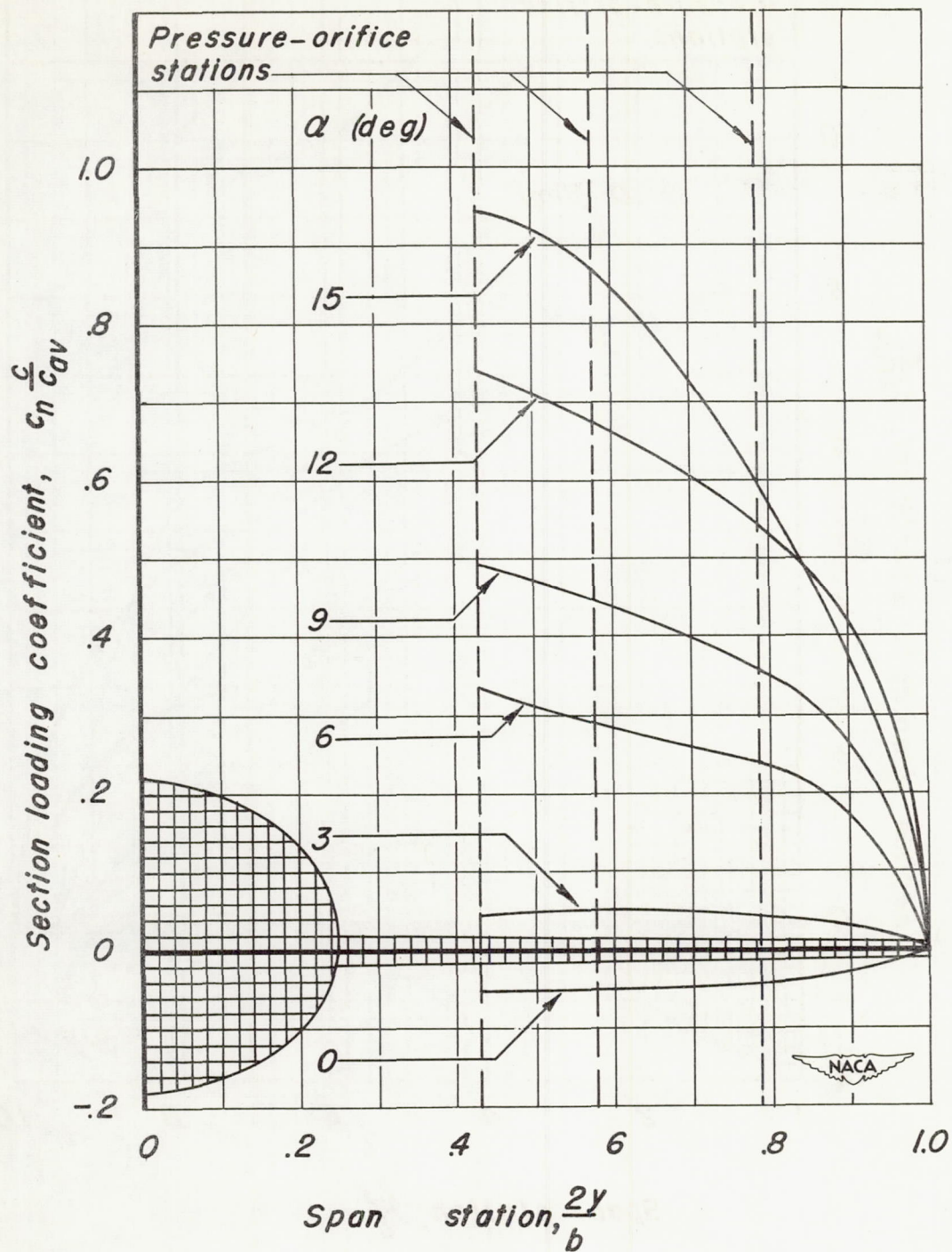
Figure 13.—The spanwise distribution of load on the wing of the X-3 model.  $\psi_u, 0^\circ$ ;  $\delta_{lf}, 30^\circ$



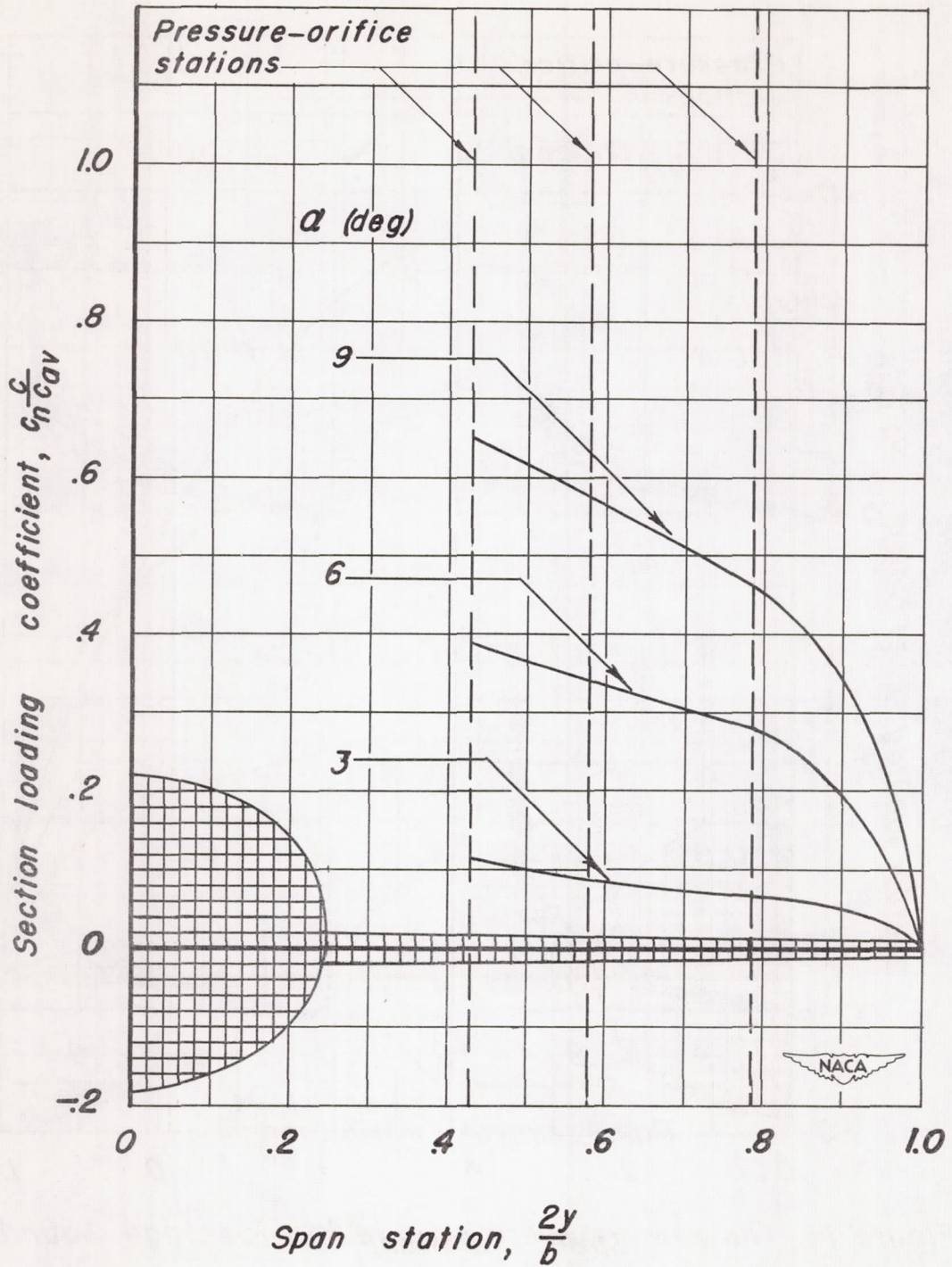
(b) Mach number, 0.60.  
Figure 13.—Continued.



(c) Mach number, 0.80.  
Figure 13.-Continued.



(d) Mach number, 0.90.  
Figure 13.-Continued.



(e) Mach number, 0.925.

Figure 13.-Concluded.

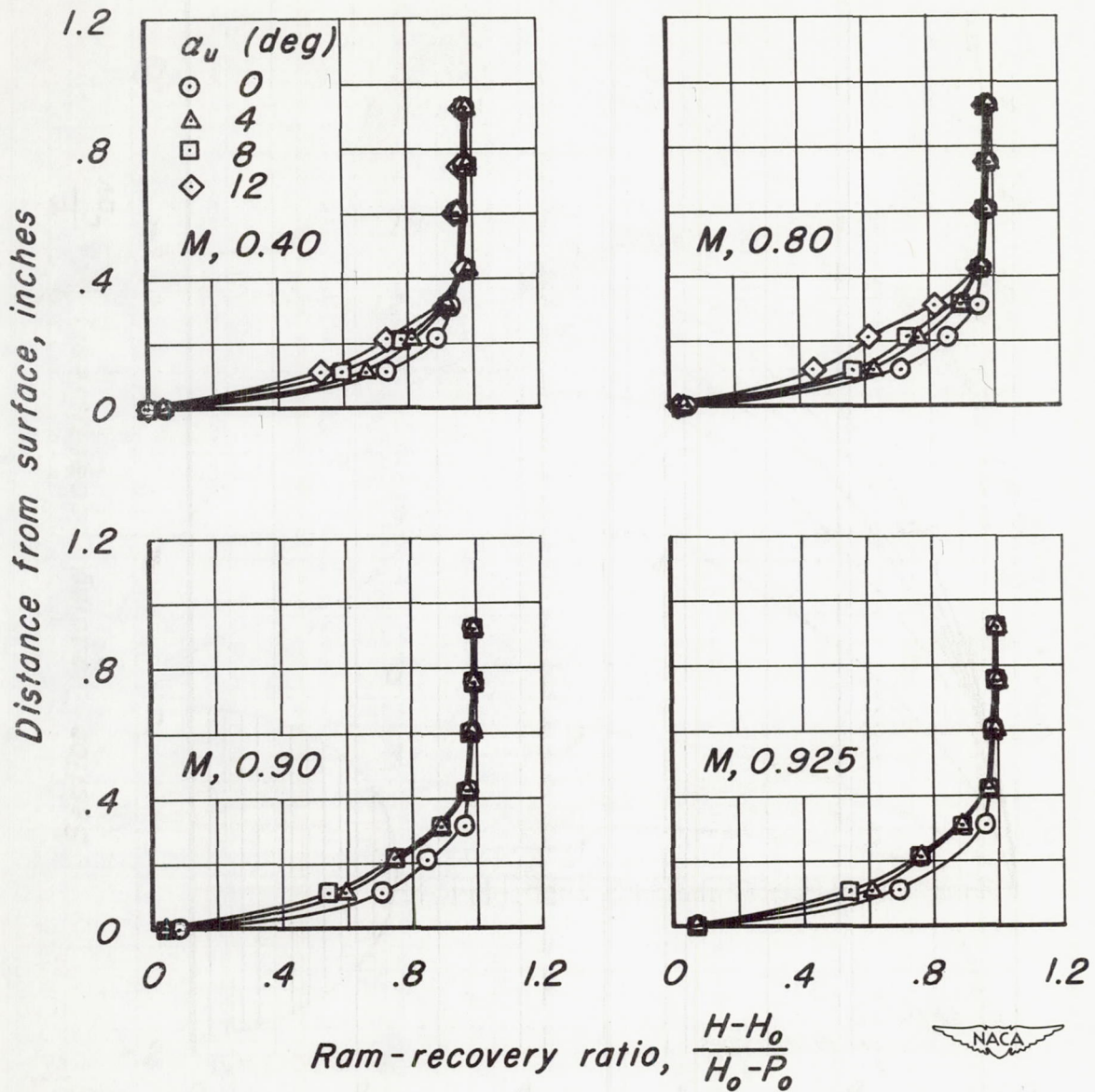
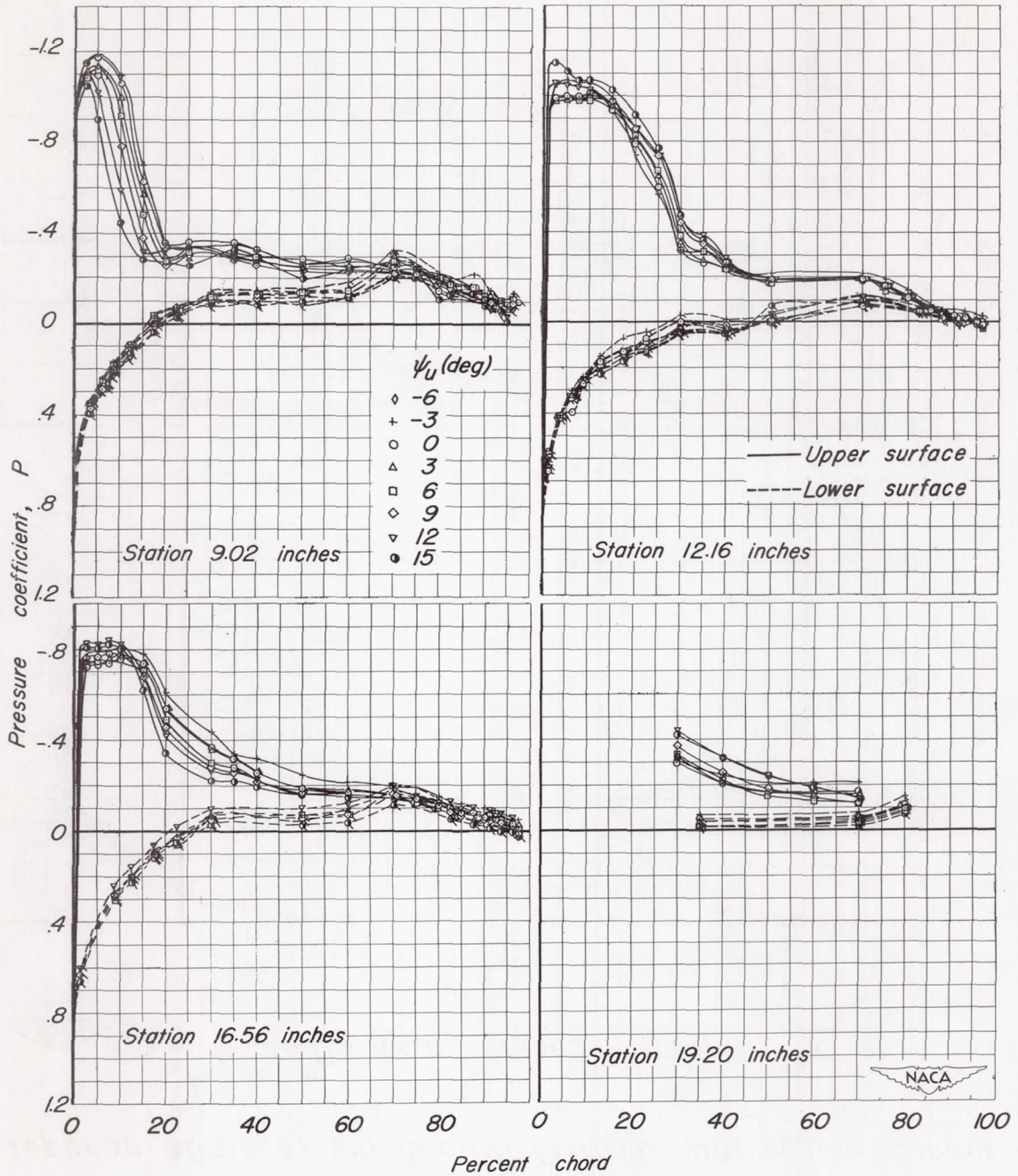
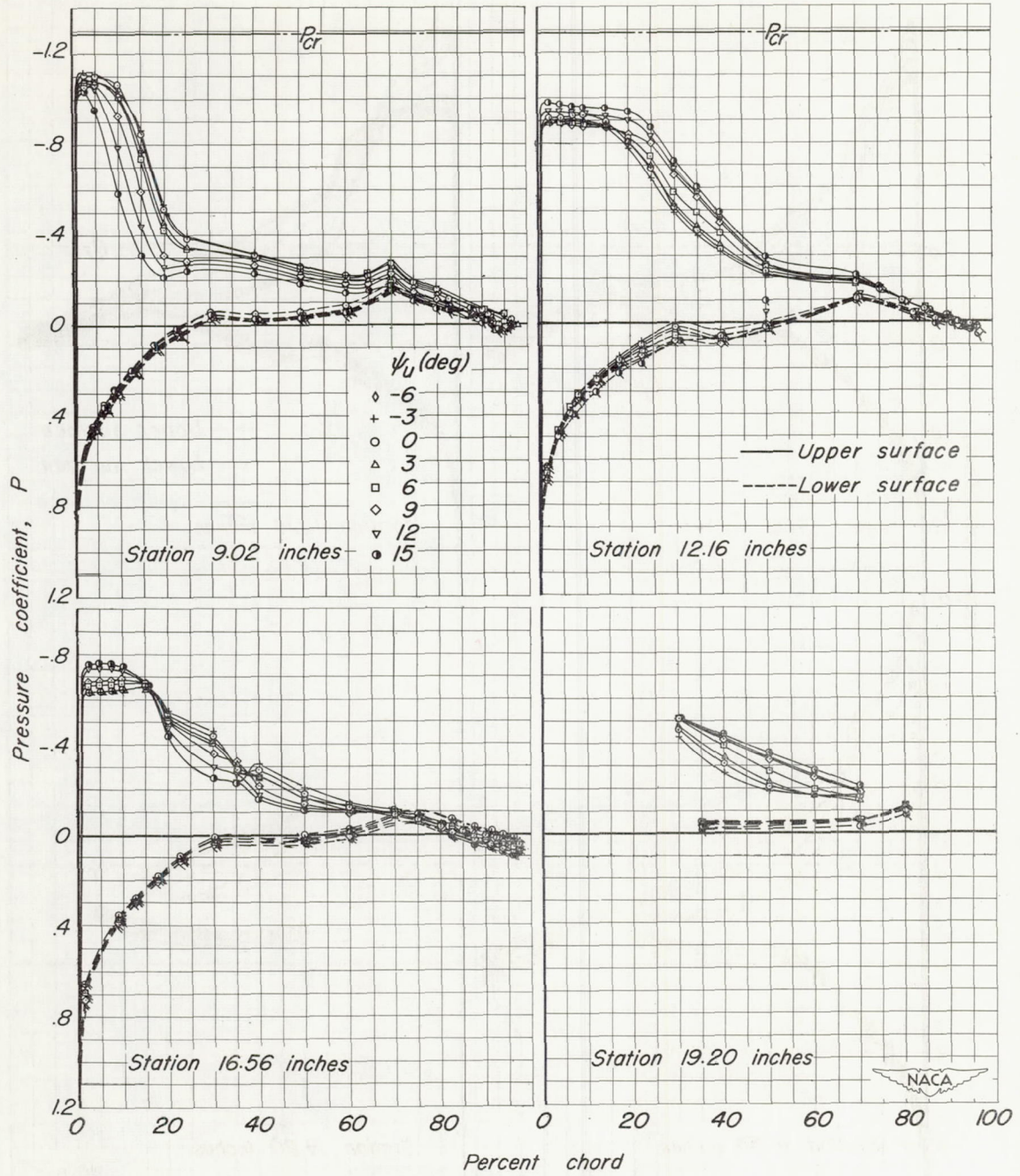


Figure 14.—The ram-recovery ratio in the fuselage boundary layer of the X-3 model at station 43.2 inches.  $\psi_u, 0^\circ$



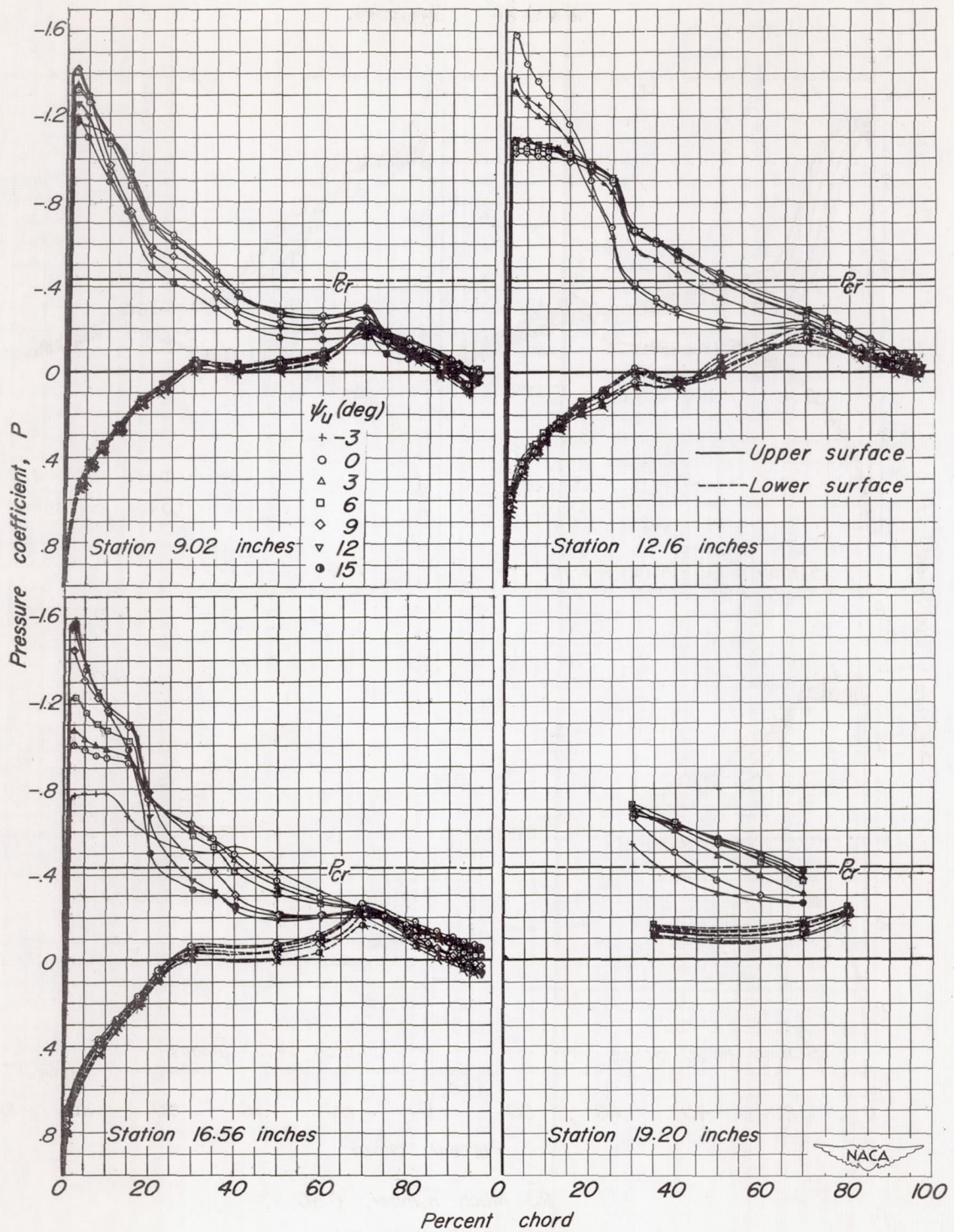
(a) Mach number, 0.40.

Figure 15.—The pressure distribution over the wing of the X-3 model.  $\alpha_u, 6.2^\circ$ ;  $\delta_{lf}, 0^\circ$



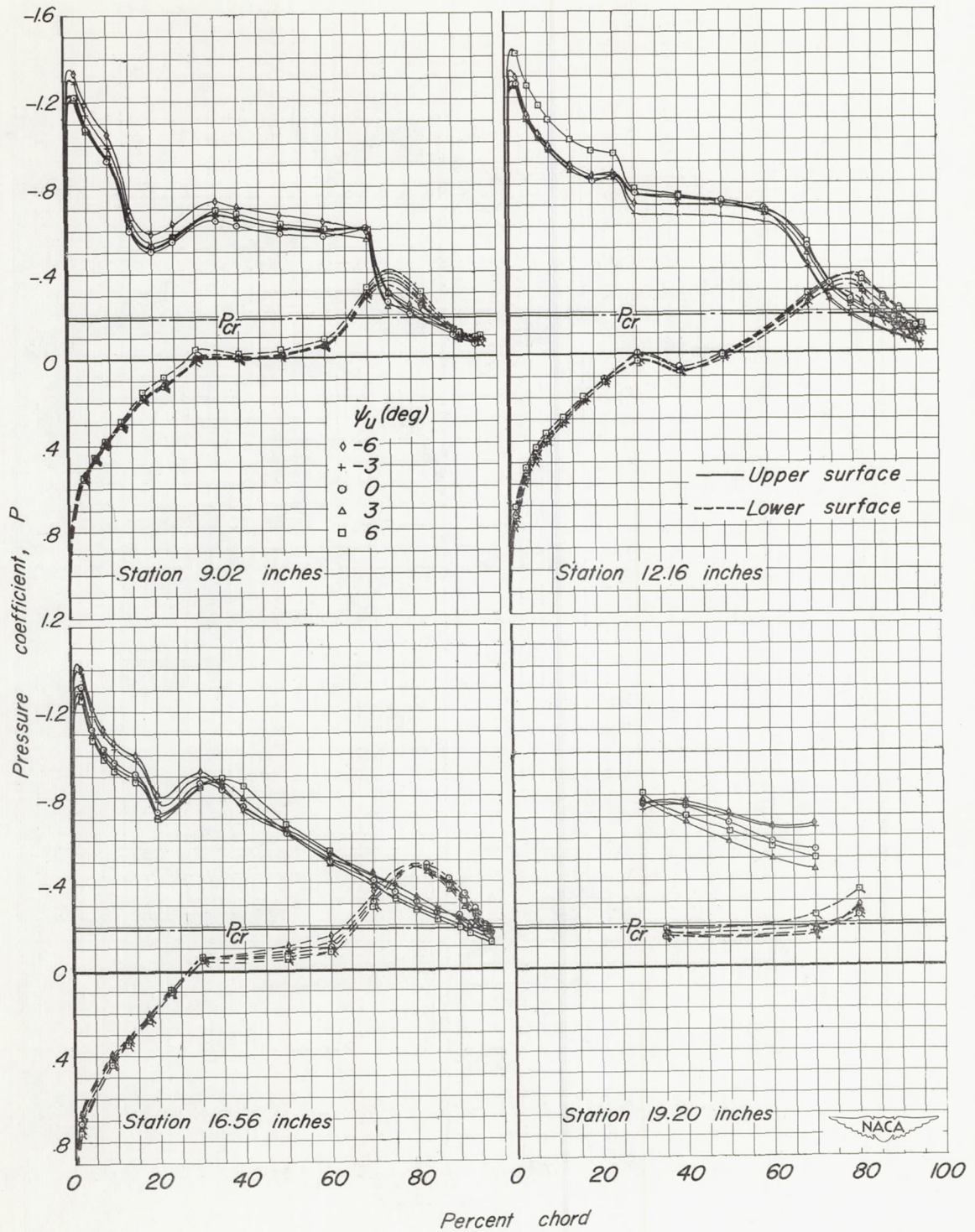
(b) Mach number, 0.60.

Figure 15.—Continued.



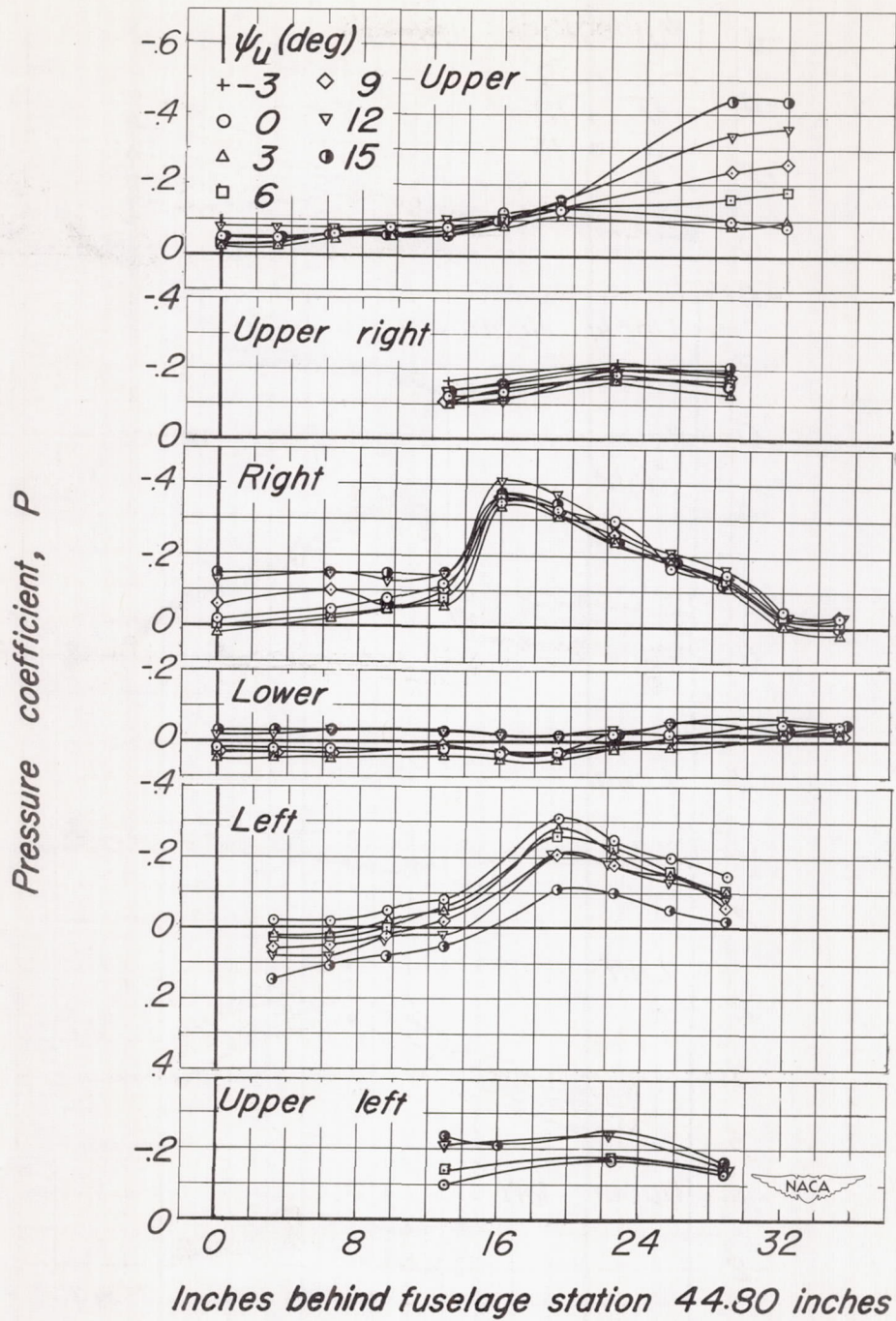
(c) Mach number 0.80.

Figure 15.—Continued.



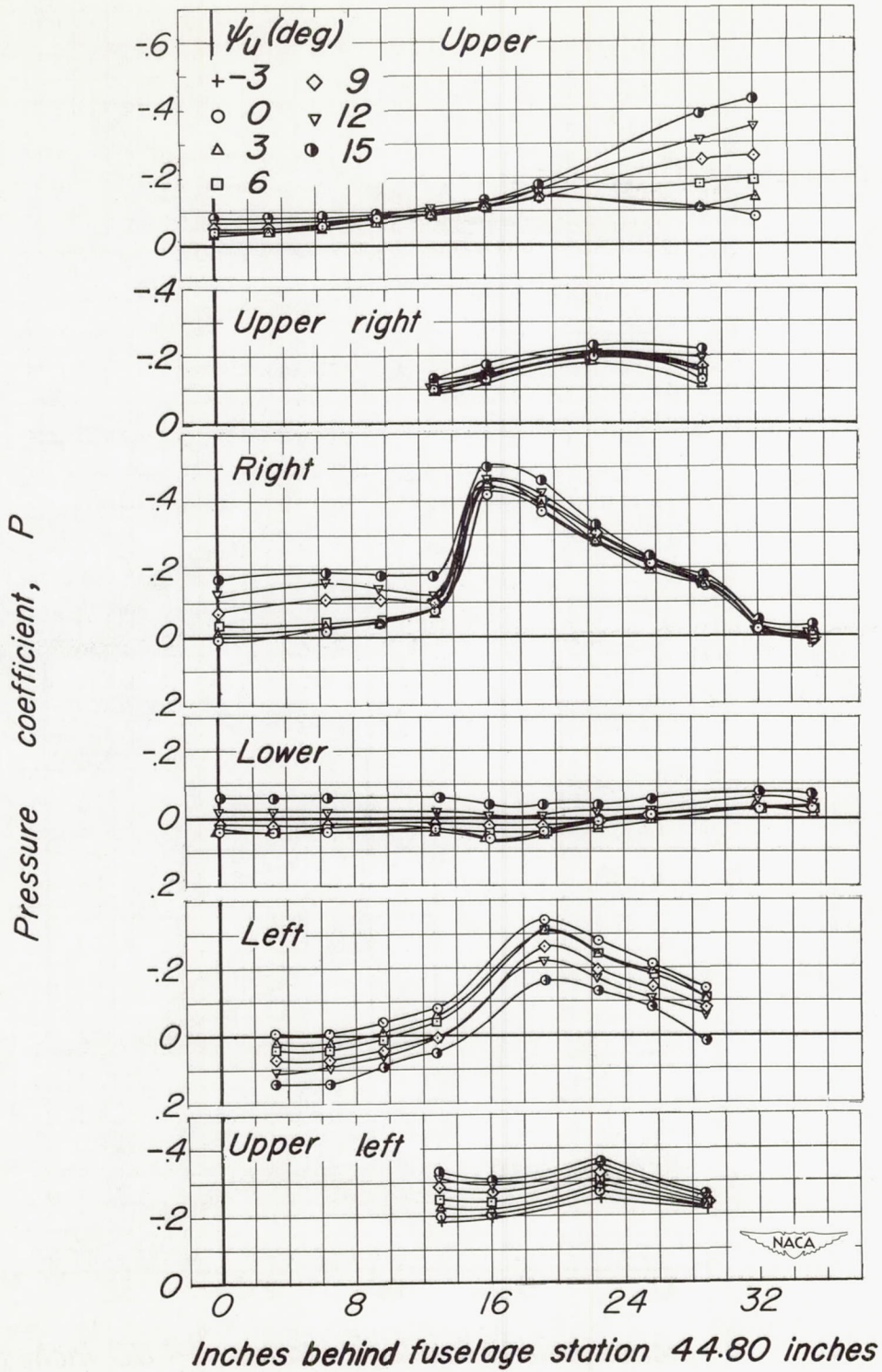
(d) Mach number, 0.90.

Figure 15.—Concluded.

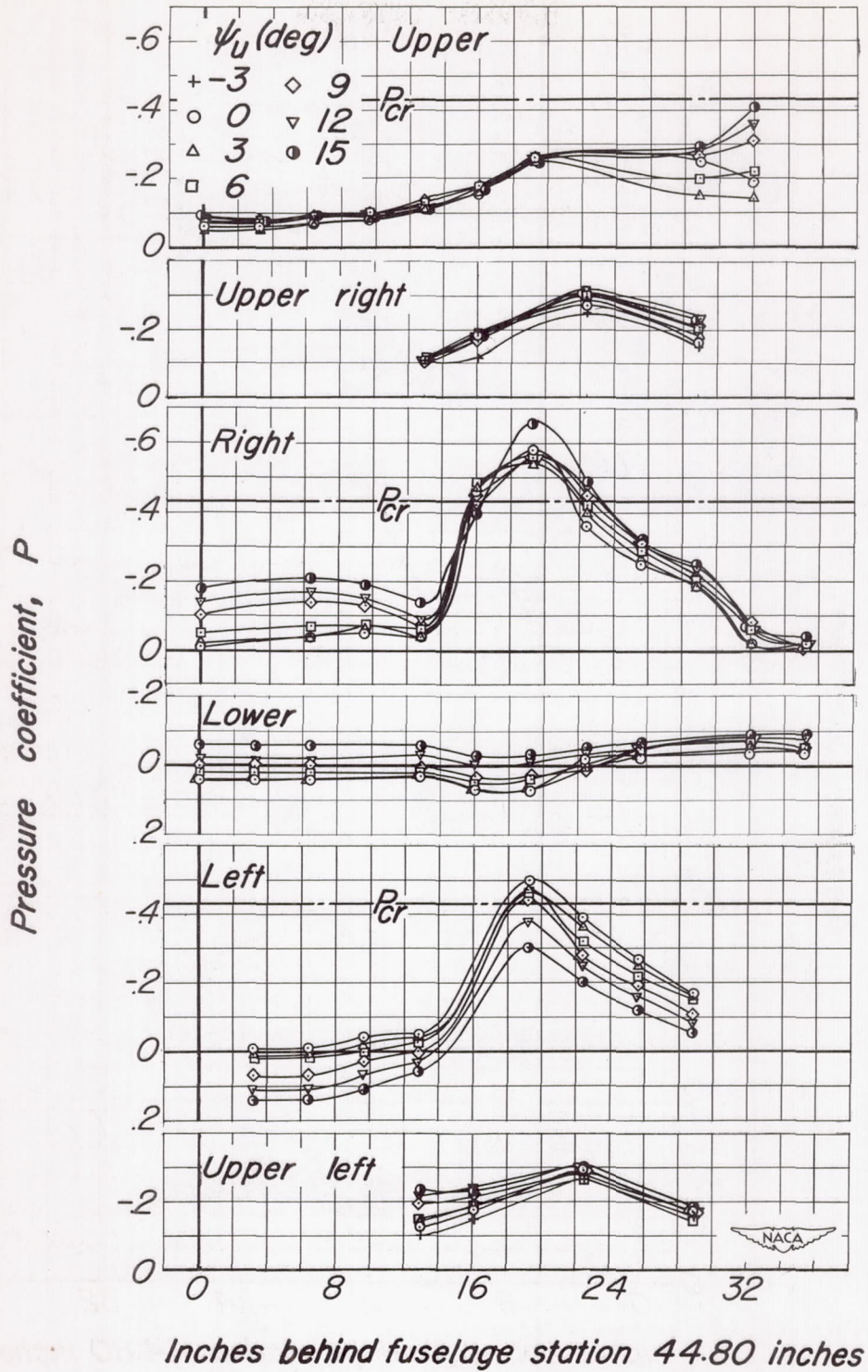


(a) Mach number, 0.40.

Figure 16.—The pressure distribution over the fuselage of the X-3 model.  $\alpha_U, 6.2^\circ$ ;  $\delta_{lf}, 0^\circ$

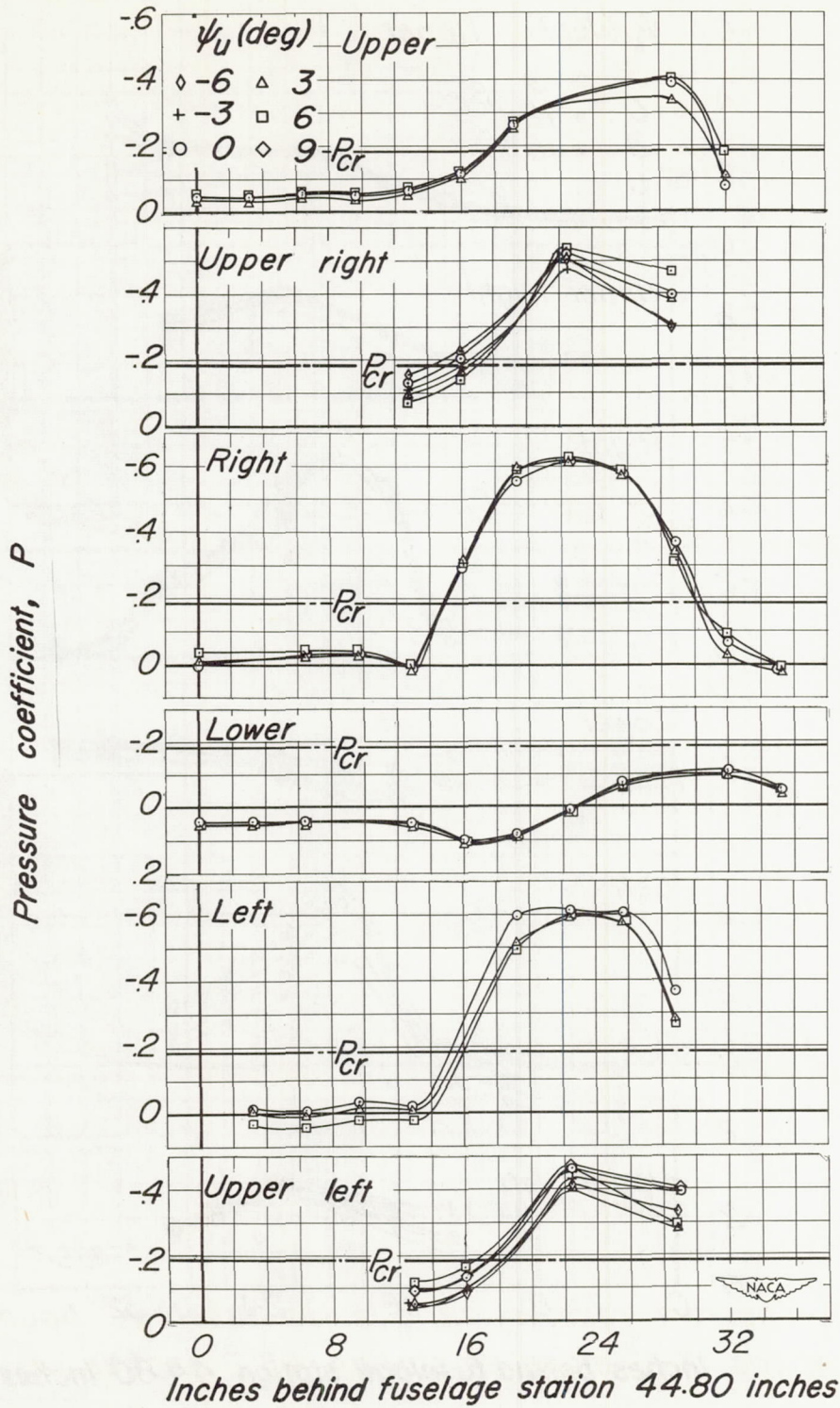


(b) Mach number, 0.60.  
Figure 16.-Continued.



(c) Mach number 0.80.

Figure 16.—Continued.



(d) Mach number, 0.90

Figure 16.-Concluded.

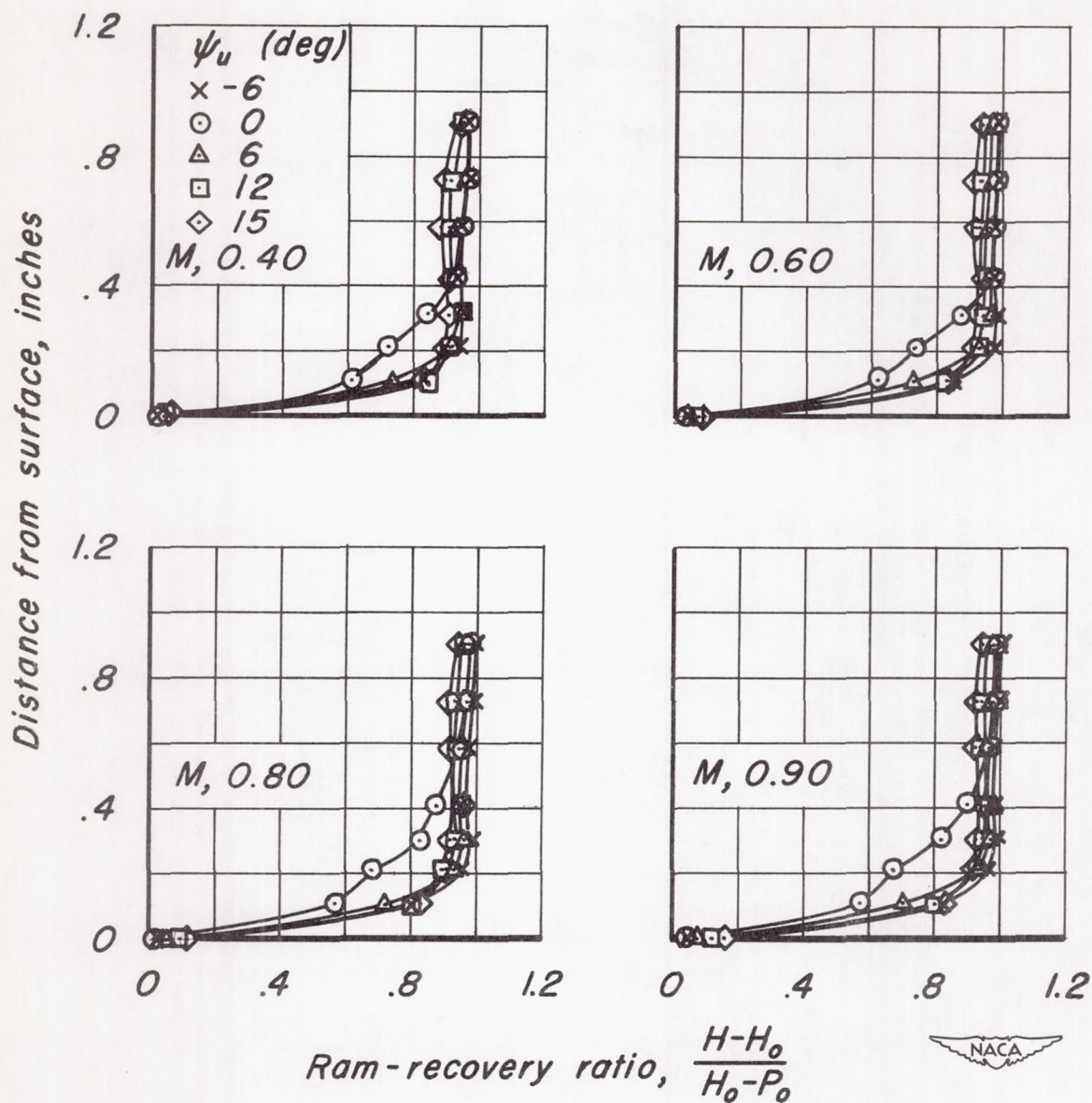


Figure 17.—The ram-recovery ratio in the fuselage boundary layer of the X-3 model at station 43.2 inches.  $\alpha_u, 6.2^\circ$

